Rijksuniversiteit Groningen

Bachelor Thesis

Determining Resonances of Stellar Streams in the Milky Way halo

A study on regular, resonant and chaotic orbits of stellar streams

rijksuniversiteit groningen

Author:
H. Posthumus

Supervisors:
A. Helmi
H.C. Woudenberg

Abstract

Stellar streams are formed by tidal stripping of globular clusters and dwarf galaxies in the Milky Way Potential. They serve as a powerful tool to constrain the properties of the potential of the Milky Way halo. In this thesis, we integrate stellar streams in a Milky Way potential including a triaxial dark matter halo. We focus on streams that are at a distance >15 kpc today, and determine their dynamical category: regular, resonant or chaotic. We find that 4 out of 25 streams are on a resonant orbit: 300S, C-12, Elqui and NGC 7492. There are also 4 out of 25 which have a Lyapunov exponent >0, indicating they are on a chaotic orbit: NGC 1261, NGC 1851, NGC 2298, Tucana III. All other streams we studied are on a regular orbit.

Acknowledgements

First of all, I would like to thank Prof. Dr. Amina Helmi and Hanneke Woudenberg for guiding me through my first hands-on science experience. They truly taught me a lot, including being critical of my data and results, and kept me on the right track during these past three months.

Secondly, I would like to thank Sabine van den Brom for the mutual support throughout our similar theses.

Lastly, I would like to thank my parents, sister, friends, and partner for always supporting me during my bachelor programme and thesis period.

For this thesis, ChatGPT was used for troubleshooting coding errors.

Contents

1 Introduction

In the late 90s and early 2000s, the first stellar streams were discovered, namely the Sagittarius dwarf galaxy (Ibata et al. (1995)), the Helmi streams (Helmi et al. (1999)) and the Palomar 5 globular cluster (Odenkirchen et al. (2001)). Since then, other stellar streams were discovered, and in the Gaia era (from 2017 onwards), the number of spatially coherent stellar streams reported in literature has reached over 120, with the number ever-increasing using more modern methodologies and technologies (Bonaca & Price-Whelan (2024)). Obtaining reliable and robust data of stars is key to identify the membership of stars to certain streams. The Gaia mission has made this possible by measuring the positions and motions of almost two billion stars in the Milky Way (Gaia Collaboration et al. (2017), Gaia Collaboration et al. (2018), Gaia Collaboration et al. (2023)), with even more data to come in the future. The data that we use in this thesis is based on Gaia data (see section 2).

Stellar streams are formed by the tidal stripping of stars from globular clusters or dwarf galaxies if the Milky Way potential is sufficiently strong. Because the process of tidal stripping is common, the shape and behaviour of these stellar streams is similar (though the orbits of the streams may look radically different, depending on their initial conditions). On the other hand, they also look different, which is due to the different properties of globular clusters and dwarf galaxies. Dwarf galaxy streams tend to be longer, wider, and smoother than globular cluster streams (Bonaca & Price-Whelan (2024)).

There is a number of ways that stellar streams are discovered. For example, `streamfinder` (Malhan & Ibata (2018)) searches for over-densities of stars near orbits computed assuming a model for the Milky Way's mass distribution. This is done by projecting orbits into the data space. Other methods include clustering methods where the distribution of phase-space of candidate members is measured (Necib et al. (2020), Gatto et al. (2020)), or machine learning methods and anamoly detection methods are applied (Borsato et al. (2020), Shih et al. (2022), Pettee et al. (2024)).

The dynamics of stellar streams are of interest to study, because they are a powerful tool to constrain the properties of the potential of the Milky Way halo (e.g. Posti & Helmi (2019), Dodd et al. (2022), Palau & Miralda-Escudé (2023)). Particularly its shape (Vera-Ciro & Helmi (2013), Vasiliev (2021)), its mass (Bovy et al. (2016), Malhan & Ibata (2019)) and its radial density profile (Gibbons et al. (2016)). Next to constraining the potential of the Milky Way halo, streams are also a promising method to reveal dark matter subhalos, which are expected to orbit galaxies in large numbers in the case they are cold (Moore et al. (1999), Klypin et al. (1999)). Those halos could produce gaps, overdensities, and off-stream features in stellar streams (Yoon et al. (2011), Erkal et al. (2016), Bovy (2016), Koppelman & Helmi (2021)). For example, the off-stream features in GD-1 are thought to have been caused by an unknown structure orbiting close to the plane of motion of the Sagittarius dwarf galaxy, with a mass of $10^6\ M_\odot$ (Bonaca et al. (2019)).

We can distinguish between three main dynamical categories of orbits that streams can be on within a potential: regular, resonant and chaotic orbits (more on this in section 3.3). Streams on a resonant orbit are easier to detect, since they stay coherent for longer as they phase mix slower. Streams on regular non-resonant orbits phase mixes at a rate $\propto t^{-3}$, where t is time, streams trapped by a resonant orbit phase mix slower, at a rate $\propto t^{-2}$ for a singly resonant orbit and at a rate $\propto t^{-1}$ for a doubly resonant orbit (Vogelsberger et al. (2008)). Thus, there might be a bias towards detecting resonant orbits. On the other hand, streams on chaotic orbits will diffuse much faster, as their orbits diverge exponentially in time.

In this thesis, we will be studying a set of 25 stellar streams that are observed to be >15 kpc

from the Galactic center. Specifically, we will integrate the initial conditions of the streams and determine which streams are on a resonant, chaotic or regular orbit. The streams that we will be studying are shown in a Mollweide plot in figure 1. The structure of this thesis is as follows. Section 2 discusses the data used in this paper, based on Gaia data. Section 3 discussed the methods used to determine whether an orbit is (near-)resonant, chaotic or regular. In section 4, we show our results. Section 5 discusses the results and the limitations of the work. In section 6 we show our conclusions.

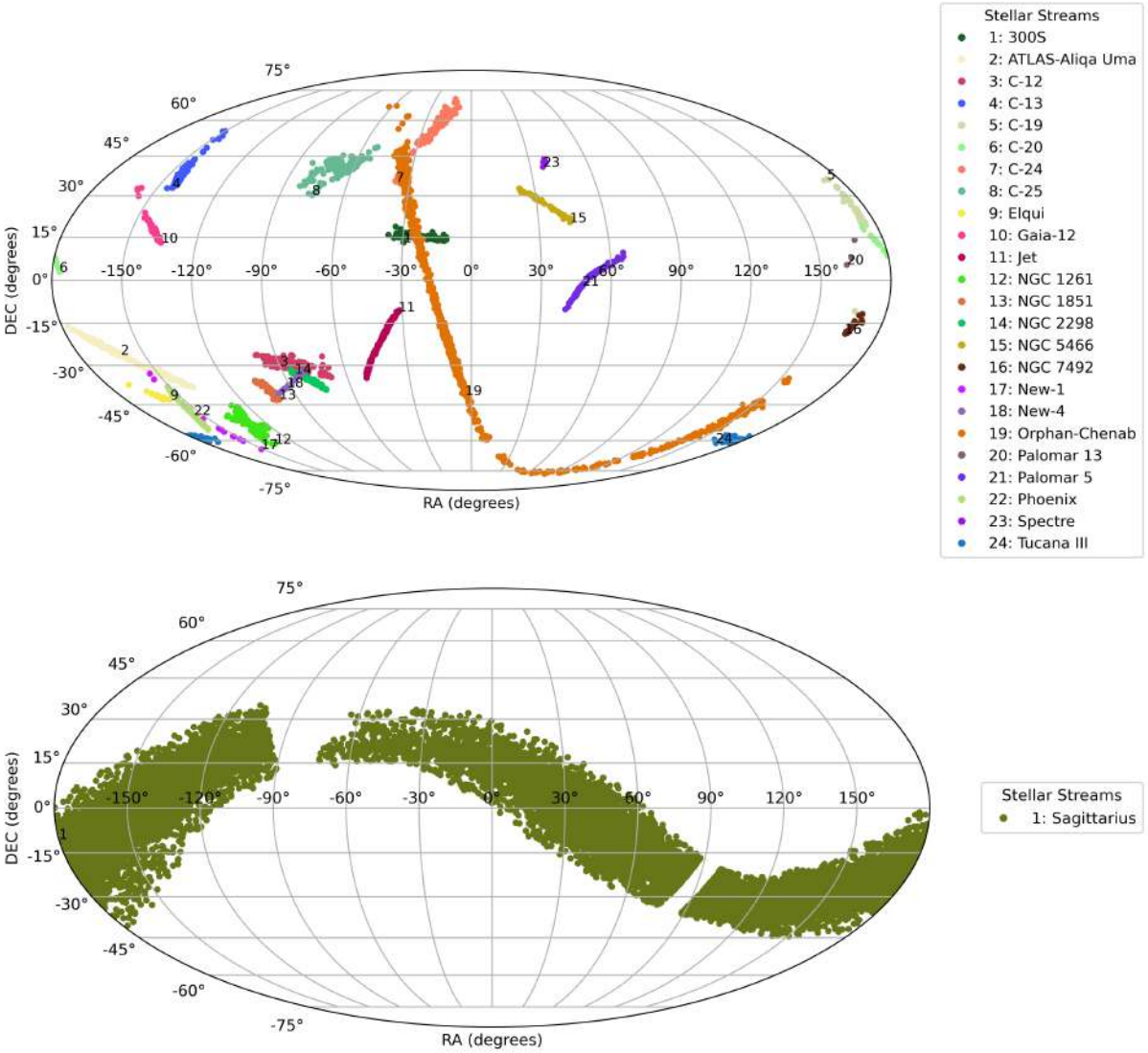

Figure 1: Two Mollweide plots of all streams that we will be studying. To avoid confusion, the stream Sagittarius is plotted in a different plot, since it spans a big area and by far contains the most stars. All streams are numbered in the plot, and the names of the respective numbers are shown in legends on the right.

2 Data

2.1 A compilation of stream's data

We use data from Bonaca & Price-Whelan (2024), who list a total of 131 streams, which can be found on a Github repository[1]. 92 of these 131 streams have measured stellar data from Gaia DR3 for the corresponding stream candidates. Some of these stream candidates were assigned to a stream using `streamfinder` (Malhan & Ibata (2018)), which were found using overdensities of stars. For all 131 streams, the on-sky width and length is reported, as well as the heliocentric and Galactocentric distances (median distances from the `galstreams` track (Mateu (2023))) and the pole and origin of the stream's reference frame (also obtained from `galstreams`). The dataset comprises the observables of each stream in ICRS (International Celestial Reference System) coordinates (R.A., Dec., R_{helio}, proper motion in R.A. and Dec., V_r) and the inferred orbital parameters. The way the observables and the inferred orbital parameters are obtained is as follows. The candidate members of each of the 92 streams are transformed to a stream-rotated coordinate system. The most likely best-fitting initial conditions of the stream (R.A., Dec., R_{helio}, R.A. and Dec proper motions, V_r) were inferred by setting one fixed point (ϕ_1), which is typically close to the center of the stream. The orbit is then integrated multiple times in the `MilkyWayPotential2022` from the `gala` package (Price-Whelan (2017)), using a set of free parameters, also in the stream rotated coordinate system (ϕ_2, D, μ_{ϕ_1}, μ_{ϕ_2}, v_r). The log-likelihoods of all orbits are calculated using cubic interpolation. The orbital control points of the streams was set using the most likely fit, at the aforementioned fixed point (ϕ_1). From these orbital control points, other orbital parameters were computed, assuming the potential of Price-Whelan (2017).

We need the orbital control points of the stream, as we will use them as our initial condition when we integrate orbits of the streams (see section 3.1).

2.2 Stellar data

Besides using the best-fitting initial condition of each stream, we also use the data of individual candidate member stars of each stream reported in Bonaca & Price-Whelan (2024) to integrate stars directly from their measurements, rather than from an inferred initial condition. We do this such that we can later compare our results of the integrated orbit from the initial condition to the orbit of the stream candidates. This stellar data comes from a range of different sources on Gaia-based studies: Awad et al. (2024), Bonaca et al. (2020), Chandra et al. (2022), Ferguson et al. (2021), Grillmair (2019), Grillmair (2022), Huang et al. (2019), Ibata et al. (2024), Koposov et al. (2023), Li et al. (2021), Shipp et al. (2020), Shipp et al. (2019), Yang et al. (2022), Yang et al. (2023), Vasiliev et al. (2021). The relevant properties for us that are reported are the observables of the stars (R.A., Dec., R_{helio}, proper motion in R.A., proper motion in Dec., V_r) in ICRS coordinates, and their errors. One complication is that for many stars, there is no distance measurement, and for some of them, there is also no V_r measurement. This issue will be addressed in section 3.4.

2.3 Solar constants

We need to transform our initial conditions from ICRS coordinates to Cartesian Galactocentric coordinates, so we can integrate them in a potential that is defined around the Galactic center. For this, we assume the following properties of the Sun: $R_\odot = 8.122\,\mathrm{kpc} \approx x_\odot$ (Abuter et al.

[1] https://github.com/abonaca/streams_overview

(2018)), the height above the midplane $z_\odot = 0.025$ kpc (Jurić et al. (2008)). We use a left-handed Galactocentric coordinate system. Since the Sun is aligned with our coordinate system, we assume that $y_\odot = 0$ kpc. To correct for the motion of the Sun, we use the proper motion of Sagitarrius A* (Reid & Brunthaler (2004)) and the following relation (Woudenberg & Helmi (2024)):

$$v_j = 4.74057\,\text{km s}^{-1}(\frac{\mu_j}{\text{mas yr}^{-1}})(\frac{\text{d}}{\text{kpc}}).$$

Here, j=(l,b), which stand for galactic longitude and galactic latitude respectively and d is the distance to the Sun from the Galactic center. Using this relation, we get the following peculiar velocities: $V_\odot = 245.6$ km s^{-1}, $W_\odot = 7.8$ km s^{-1}. We assume that $U_\odot = 11.1$ km s^{-1} which agrees with multiple (recent) measurements (e.g. Tian et al. (2015), Mróz et al. (2019), Zbinden & Saha (2019)).

2.4 Importing and transforming the data

We import the orbital initial conditions of 92 stellar streams, which were specified in the ICRS coordinates (see section 2.1). We delete the streams that have a difference of >19% between the inferred distance (see section 2.1) and the reported heliocentric distance, which is the median heliocentric distance of the `galstreams` track. The greater difference implies that the measurements of the streams are less reliable, hence we removed those. Now, we are left with 82 streams.

We transform the initial conditions from the ICRS coordinates to Cartesian Galactic coordinates using `astropy.coordinates` (Robitaille et al. (2013)), as follows:

```
# Creating a SkyCoord object with all our ICRS data points
coords_hc = SkyCoord(ra=ra_dat*u.deg, dec=dec_dat*u.deg, distance=r_dat*u.kpc,
    pm_ra_cosdec=pm_ra_cosdec_dat*u.mas/u.yr, pm_dec=pm_dec_dat*u.mas/u.yr,
    radial_velocity=rad_v_dat*u.km/u.s, frame = 'icrs')
icrs_Galactic = coords_hc.transform_to(coord.Galactic) #transforming it to
    Galactic

# Getting the cartesian positions and velocities
cartesian_Galactic_pos = icrs_Galactic.data.to_cartesian()
cartesian_Galactic_vel = icrs_Galactic.velocity

# Extracting all the values
x_hc = cartesian_Galactic_pos.x.value  #kpc
y_hc = cartesian_Galactic_pos.y.value  #kpc
z_hc = cartesian_Galactic_pos.z.value  #kpc

vx_hc = cartesian_Galactic_vel.d_x.value #km/s
vy_hc = cartesian_Galactic_vel.d_y.value #km/s
vz_hc = cartesian_Galactic_vel.d_z.value #km/s
```

Then, we transform to Cartesian Galactocentric coordinates by adding the solar position and velocity w.r.t. the Galactocentric frame to the respective initial conditions in the Cartesian Galactic frame.

Since we want to study streams that are observed at distances >15kpc from the Galactic Center we filter out those whose initial condition of the distance is <15kpc. The thesis of Sabine van den Brom probes streams that are observed between 10 and 15 kpc from the Galactic Center. She left out streams <10kpc, since we are interested in probing the Milky Way dark matter halo, rather than the baryonic components of the Milky Way. With this selection, we are left with 28 streams that have R >15 kpc. However, as we will see in section 3.1, three streams will be filtered

out, as they are unbound in the potential we use. Thus we will analyze a total of 25 streams. A Mollweide plot of the streams that we will be studying, colorcoded by Galactocentric distance can be found in figure 2. A plot of the Galactocentric distance distribution of the streams that we will be probing can be found in figure 3.

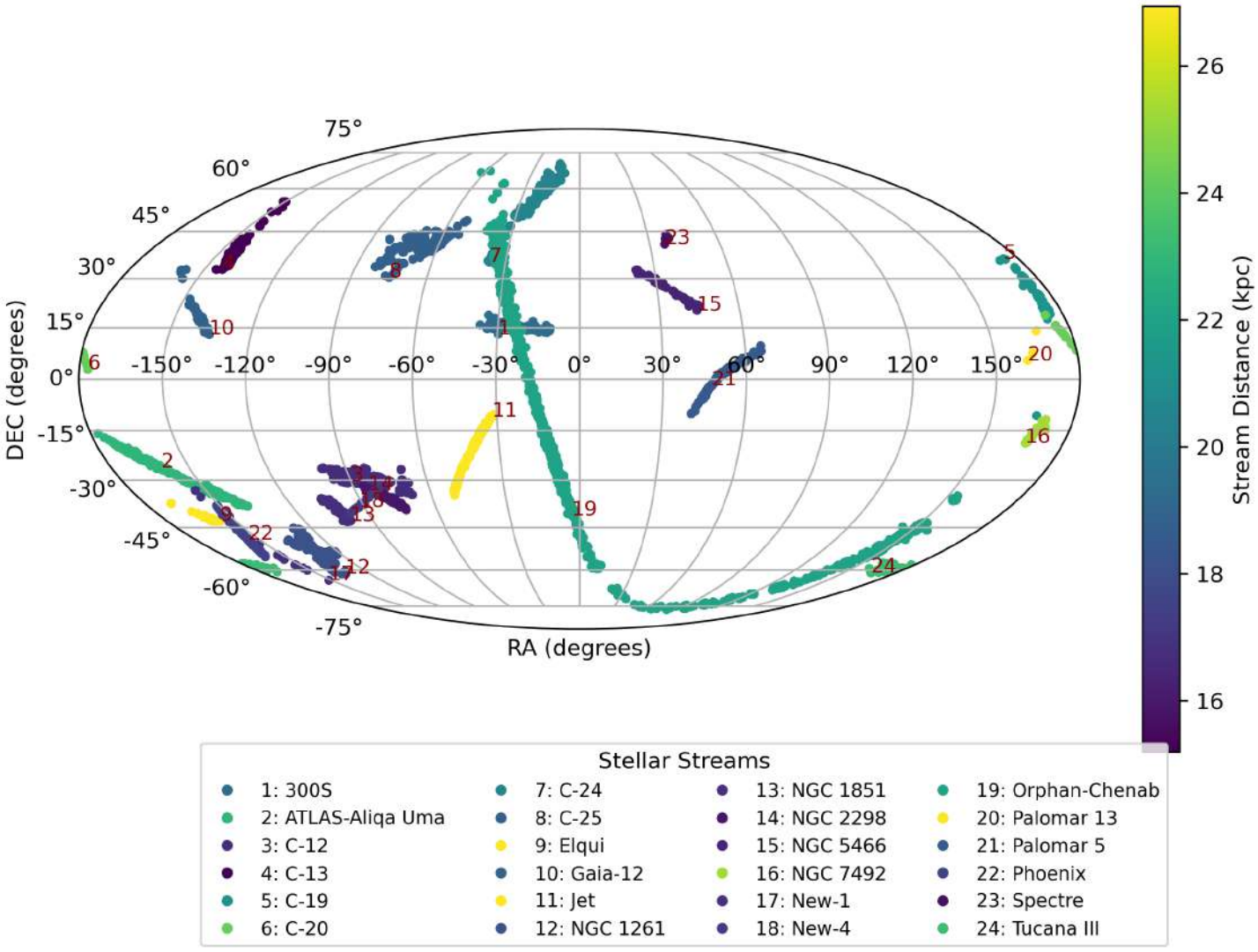

Figure 2: Mollweide plot of all streams that we will be studying, colorcoded by Galactocentric distance. Note that Sagittarius is excluded since because of two reasons. It has a relatively large distance range and galactic latitude range. Next to that, it has many stars, so other streams will become less visible. Furthermore, the two streams with the highest distance (Jet and Elqui) were left out to make the colorbar better distinguish between different streams.

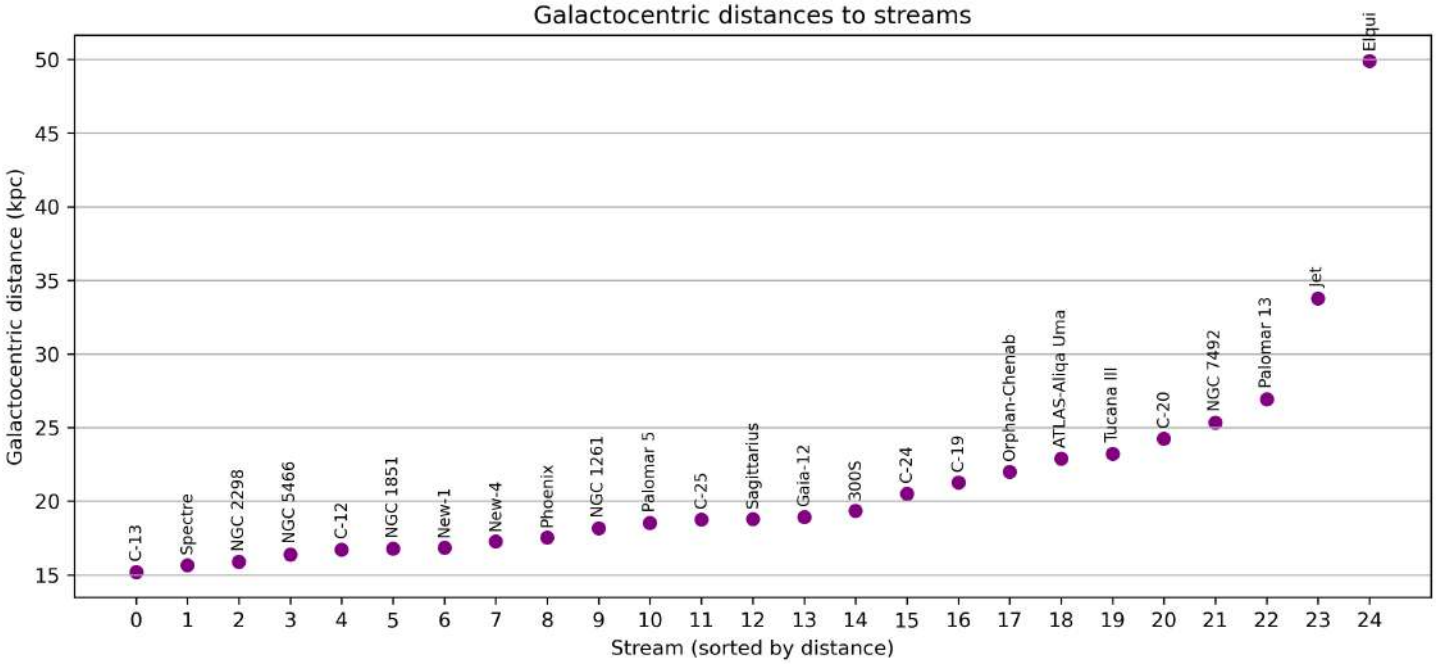

Figure 3: Galactocentric distance distribution of all streams that are studied in this work.

3 Methods

3.1 Integration of initial conditions in a Milky Way potential

We integrated the initial conditions of our sample of streams (a total of 28, see section 2) in the potential from Woudenberg & Helmi (2024). The potential consists of a bulge, a thin and thick disk, an HI gas disk, a molecular gas disk, and it is based on the potential from McMillan (2017), but instead the thick disk scale length is changed from 3 kpc to 2 kpc, and a triaxial halo that we describe below. It has a total mass of $M_{tot}(r < 20kpc) = 2.2^{+0.1}_{-0.1} \cdot 10^{11} M_{\odot}$. This potential was constrained by studying dynamical properties of the Helmi Streams (HS), specifically within 20 kpc of the dark matter halo. These properties constrain the potential up to this distance.

To constrain the potential, Woudenberg & Helmi (2024) studied the orbits of the HS in a mildly triaxial potential for the dark matter halo, where (p, q) are varied. Here,

$$p^2 = \frac{b^2}{a^2}, \; q^2 = \frac{c^2}{a^2},$$

where a is the major axis, b is the intermediate axis and c is the minor axis. The HS separate into two clumps, namely a clump with high angular momentum and a clump with low angular momentum (hiL and loL). The hiL clump has an additional substructure which is kinematically cold, because they are located close to a resonance in a range of Milky Way models Dodd et al. (2022). To constrain the potential, Woudenberg & Helmi (2024) required that the kinematically cold subclump is resonantly trapped on the

$$\Omega_{\phi} : \Omega_z = 1 : 1$$

resonance. Furthermore the model had to fit recent rotation curve data (e.g. Eilers et al. (2019)), and 40% of the loL stars is required to be on z-tube orbits. With these requirements, Woudenberg & Helmi (2024) found that $p = 1.013^{+0.006}_{-0.006}$, $q = 1.204^{+0.032}_{-0.036}$, $M_{discs} = 4.65^{+0.47}_{-0.57} \cdot 10^{10} \; M_{\odot}$, and $M_{DM}(< 15kpc) = 1.14^{+0.11}_{-0.10} \cdot 10^{11} \; M_{\odot}$.

In the potential discussed above, we numerically integrate our initial conditions using `agama.orbit` (Vasiliev (2019)). We use a function from (Woudenberg (private communication)), such that the integration conditions are a bit more intuitive, but the procedure for integrating initial conditions is still the same. The function is as follows:

```
def integrate_orbit(ic, ttot, dt, pot):
    "Integrate orbit(s) of stars with Galactocentric cartesian coordinates
        all_xyzvxyz (in kpc, km/s) for integration time ttot (Gyr) and timestep
        dt (Gyr) in potential pot."

    numsteps = abs(int(round(ttot/dt)))

    X = agama.orbit(ic         = ic,
                    potential  = pot,
                    time       = ttot,
                    trajsize   = numsteps,
                    lyapunov   = True)

    times,points = X[0].T
    Lyap = X[1]

    return times, points, Lyap
```

Initially, we set the integration time `ttot`=100 Gyr, and the output timestep `dt`=0.001 Gyr and we integrate all initial conditions (`ic`). As an output, we get the integrated orbit

(`points`), the output times of all points (`times`), and the Lyapunov exponent (`Lyap`), indicating the degree of chaos. The Lyapunov exponent measures the evolution in time of a 6D point that is infinitesimally far away from our initial condition. If the orbit is regular, the divergence of nearby orbits in configuration space grows linearly (Helmi et al. (1999), Helmi & Gomez (2007), Vogelsberger et al. (2008)), and if it is chaotic, it grows exponentially (Maffione et al. (2015), Price-Whelan et al. (2016)). If the orbit has a Lyapunov exponent >0, this indicates chaos.

Thereafter, we analyze the apocenters of the 28 integrated orbits and remove those with apocenter>300 kpc. We deem these orbits to be unbound from the Milky Way potential, and therefore we won't be able to analyze them. The following streams were excluded from the analysis for this reason: New-11, New-19 and New-25. Finally, we are left with 25 streams.

3.2 Frequency analysis

3.2.1 Integration times

To later make our frequency analysis more robust, we want to integrate all orbits for the same number of orbital periods. We determined the orbital period `T_orb` of all streams. This was defined by the average time between reaching the apocenters (Woudenberg, private communication). Then we set `N_orbits`=100, where `N_orbits` is the amount of orbits we want our integration to do. We then multiplied `T_orb` of every stream with `N_orbits` to get the integration time of every stream, and stored these as `integration_times`. Then, we integrate again and set `ttot`=`integration_time` and `dt`=`0.00001*integration_time`. With these points and times, we continue to perform our frequency analysis.

Of these 25 streams, we recover the fundamental orbital frequencies in Z, R and Ω with the package `SuperFreq` described by Price-Whelan (2015). `SuperFreq` was implemented based on the work by Laskar (1993) and Valluri & Merritt (1998). It performs a Fast Fourier Transform (FFT) on a complex time series, $w(t) + iv_w(t)$, where $w(t)$ are our spatial coordinates over time and $v_w(t)$ are our velocity coordinates over time, where our w input are Poincaré symplectic coordinates (Papaphilippou & Laskar (1996)). This FFT creates the time series of the coordinates (Z, R and Ω). The frequency with the highest amplitude is then set to be the leading frequency. Thereafter, the second and third leading frequencies are recovered, with the requirements that the coordinate of the leading frequency has to be different from the previous (two) coordinates and there needs to be a minimum difference in frequency between the different coordinates, which is set to `min_freq_diff`=10^{-6}. `nintvec` is set to 15, which is the number of frequency peaks of the spectrum that is analyzed per coordinate, choosing only the 15 peaks per coordinate with the highest amplitude. An example of such a frequency spectrum can be found in figure 4.

Using visual inspection, we noted that sometimes there is a resonance determination using frequency analysis of $\Omega_Z : \Omega_R = 1 : 2$, while using visual inspection, this was not the case. It was indeed also noted by Dodd et al. (2022), e Silva et al. (2023) and Woudenberg & Helmi (2024) that the fundamental Ω_R is not identified correctly when it is not a leading frequency. Therefore, after the frequency analysis and the resonance determination (see section 3.3), we filter out the streams which are close to a $\Omega_Z : \Omega_R = 1 : 2$ resonance according to the frequency analysis, but don't seem to have a $\Omega_Z : \Omega_R = 1 : 2$ resonance judging from visual inspection. The reason for this is that the Ω_R is sometimes determined incorrectly when it is not a leading frequency. We do the frequency analysis again for the orbits of those streams, but with a slightly different code, which removes frequencies in R that are a multiple of the frequencies in Z or ϕ (Woudenberg, private communication). This code solves the problem.

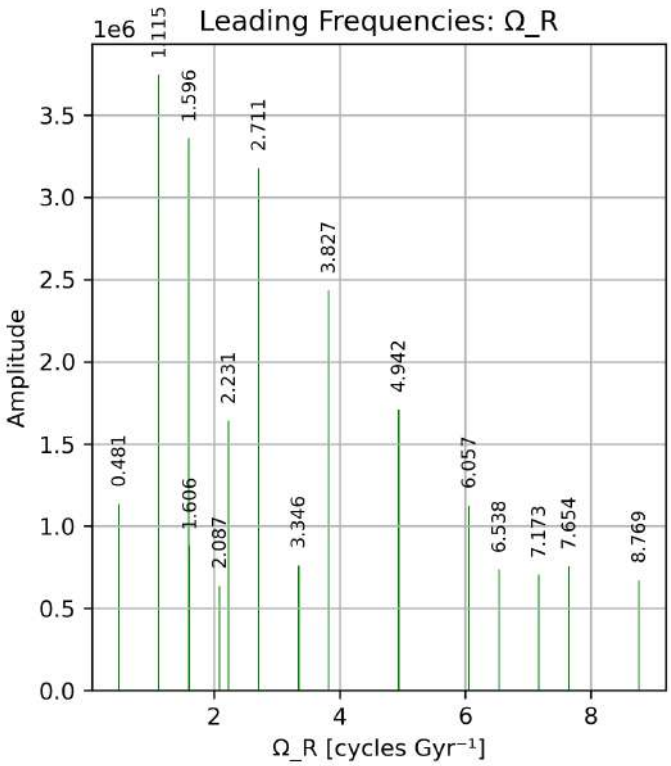

Figure 4: Example of a frequency spectrum for the stream Sagittarius

3.3 Resonance determination

In cylindrical coordinates, we typically use three orbital frequencies (Ω_R, Ω_ϕ, Ω_Z) which represent the orbit's oscillation in the radial, vertical, and azimuthal directions. We express the frequencies in units of [cycles/Gyr]. For a regular orbit, the components of its frequency spectrum are linear integer combinations of the three orbital frequencies. For a singly resonant orbit, two orbital frequencies are dependent on each other. This can be recognized by the fact that two frequencies are integer multiples of eachother, for example $\Omega_\phi : \Omega_R = 1 : 3$. For a doubly resonant orbit, all three orbital frequencies are dependent on each other, meaning all three frequencies are integer multiples of eachother. For example, $\Omega_\phi : \Omega_Z : \Omega_R = 1 : 1 : 3$. For a regular orbit, the orbital frequencies are not dependent on eachother, but they do stay constant throughout time. For a chaotic orbit, all orbital frequencies independently vary with with time.

Using these orbital frequencies, we search for low-order resonances in all streams (with low-order here, we mean resonances which have integer ratios with integers smaller than 10). We do this by using the following procedure: First, we find the frequency ratios in all streams: $\Omega_R : \Omega_Z$, $\Omega_Z : \Omega_\phi$ and $\Omega_\phi : \Omega_R$. To more intuitively see what is going on, we divide the coordinate with the highest orbital frequency by the coordinate of the lowest orbital frequency, and then make our ratio from this. For example, $\Omega_R = 4$ cycles/Gyr, $\Omega_Z = 3$ cycles/Gyr. Then $\frac{\Omega_R}{\Omega_Z} = 1.333....$ We then set our ratio to $\Omega_R : \Omega_Z = 1.333... : 1$. To figure out how close the stream is to being singly or doubly resonant, we look at the left hand side of our ratio, and looked how close it is to an low-order integer ratio. For example, our ratio is $\Omega_\phi : \Omega_R = 1.66693908 : 1$. If we multiply both sides of the ratio by 3, we get $\Omega_\phi : \Omega_R = 5.00081724 : 3$. We then define how close the left hand side is to an integer value, by setting a tolerance. If the integer value of the value on the left hand side is within the limits of this tolerance, we say it is on a resonance. For

example, $5+10^{-3}=5.001$. Since the value on the left hand side is within 5 and 5.001, we say it is on a resonance with tolerance 10^{-3}. However, it is not on a resonance with tolerance 10^{-4}. This means that the value would be on a $\Omega_\phi : \Omega_R = 5 : 3$ resonance if we set our limit to 10^{-3}, but not if we set our limit to 10^{-4}, since then the value won't satisfy `int<=value<=int+tolerance`. We also take into account the Lyapunov exponent that was determined when doing the integration, and take extra caution with our results when the exponent is greater than 0.

We also inspect the orbits visually to see if they are truly on a resonance. Since the potential we are integrating our initial conditions in is nearly axisymmetric, meaning there is a near-symmetry around the x and y axis and above and below the plane, the orbit should also be nearly axisymmetric. If it is not, this is a very good indication that it is resonant, since it reacts less strongly to the symmetry of the potential and follows the resonance. Another good indicator for resonances, is that they follow the same orbit over and over, creating overdensities in the space they occupy over time.

3.4 Analysis of individual stars

To get more robust results, we additionally determine whether the orbits of the stream members are resonant or not for a subset of the stars in each of the streams in our sample. We use a similar, but slightly different methodology as before.

We import the coordinates of stream candidates for our 25 streams. Some candidates of the streams only have 4D information (no distance and radial velocity information), so we filter these out (Jet and Palomar 13). For the streams with candidates that have 5D information, we identify the twenty points (stars) that have the shortest Euclidean distance in R.A. vs Dec. space to the initial condition used to integrate the stream. Of these twenty points, we determine the 5 points (stars) that have the shortest Euclidean distance in proper motion space to the initial condition used previously, and use those points to integrate. If there are less than 5 stars in a stream with 5D information, we use all the candidate members to integrate, and additionally, we sample points within the errors of the 5D data using `np.random.normal`. We pick the candidate member to sample from randomly, using `np.random.choice`. This process is being repeated until we have 5 sampled 'stars'. We assign a distance to them using the distance from the initial condition of the orbital control point of the stream, within a 5% error, using `np.random.normal`. For data which has tentative members with 6D information (which is only Sagittarius), we do a similar thing, except we assign their measured distance. Then, all these points are transformed to Cartesian Galactocentric coordinates in the same way as before.

When integrating the initial conditions using individual stars, we are almost doing the same thing as before, except we use the integration times that were found in section 3.2.1, assuming that the orbital period does not differ by much. The frequency analysis and resonance determination is done in the same way.

3.5 Check with stellar data points

To check if our orbit integrations went well and if we can rely on them, we transform all the points obtained from the orbit integration back to ICRS coordinates by doing the reverse procedure described in section 2.4. We check if the integrated initial conditions match the integrated initial conditions for the streams in RA and DEC, and for completeness we also show the initial conditions for our integrations of the stream and the candidate members, which can be found in figure 5. In figure 6, we show the same graphs, but zoomed in on the stellar data. This data also better shows the spread of initial conditions for tentative members.

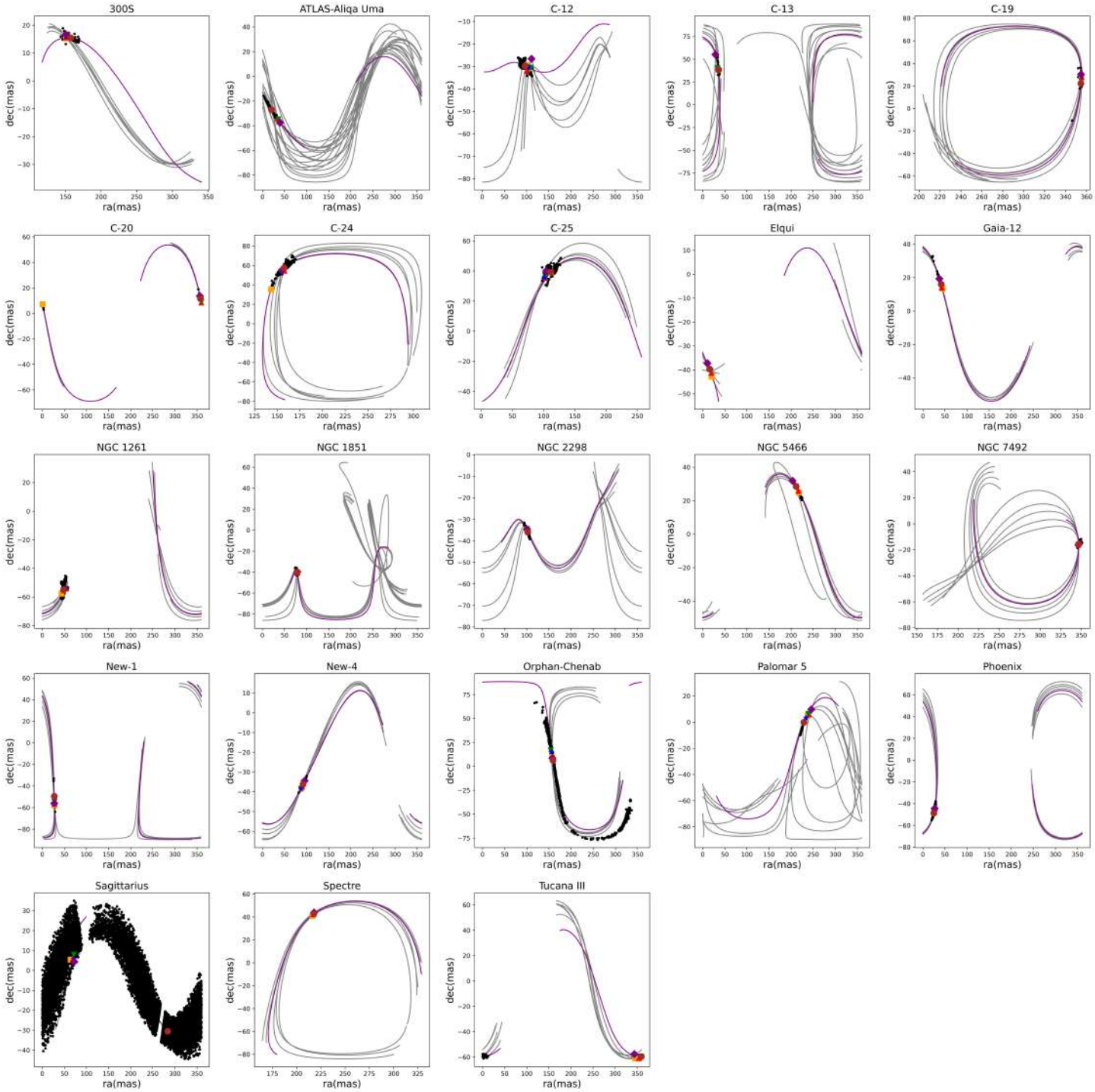

Figure 5: Right Ascension vs Declination for all data which has stellar 5D or 6D velocity. The stellar data (black scatter), initial conditions (colored scatter), orbit of the stream's initial condition (purple), and orbit of the candidate members (grey) is shown

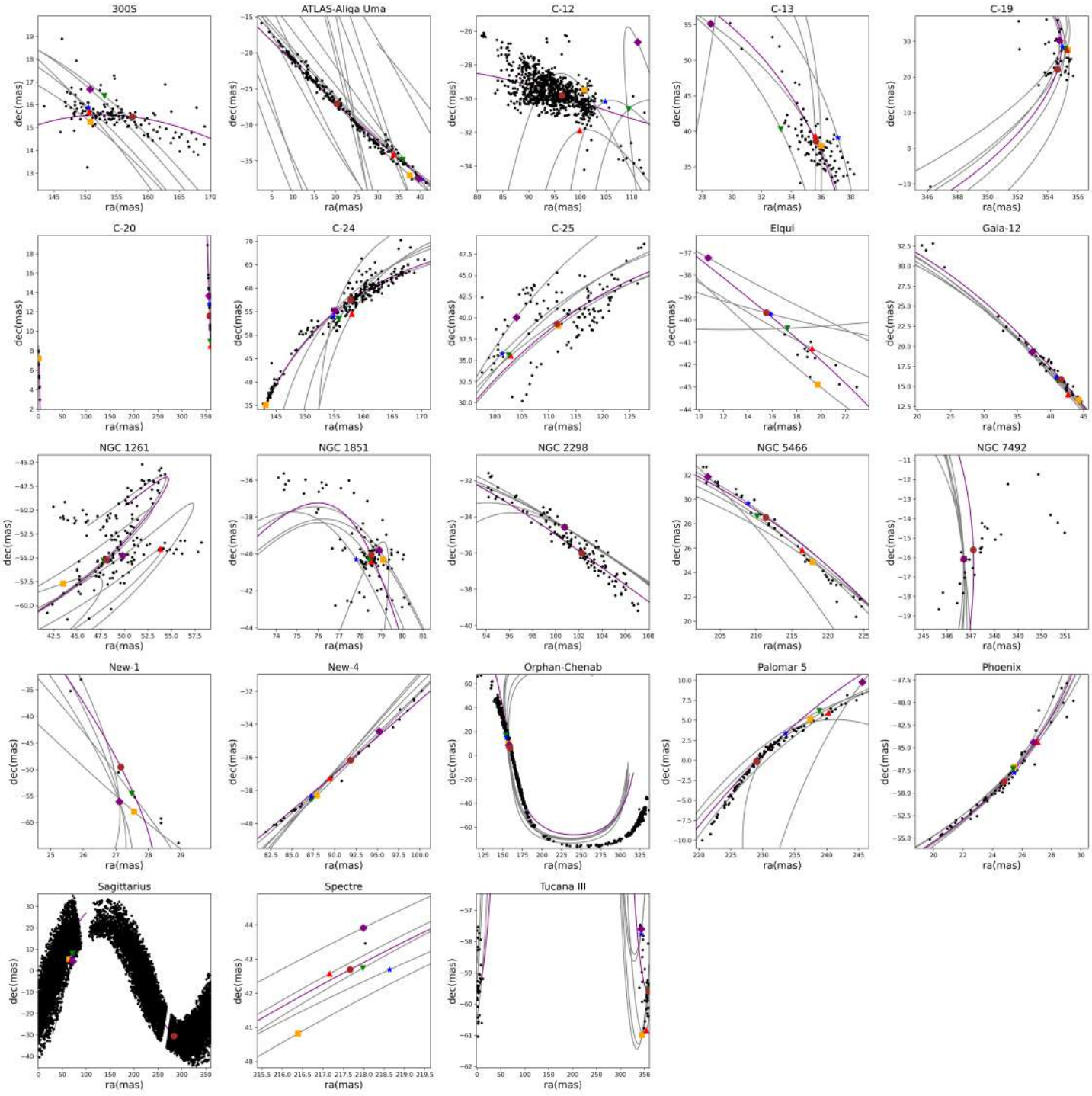

Figure 6: Right Ascension vs Declination for all data which has stellar 5D or 6D velocity, zoomed in on the candidate members of the corresponding stream. The stellar data (black scatter), initial conditions (colored scatter), orbit of the stream's initial condition (purple), and orbit of the candidate members (grey) is shown

4 Results

Table 1 summarizes the results of the resonances determined by frequency analysis, with different tolerances. It also checks whether these resonances seem to be correct, judged by our visual inspection. In the 'name' column of the table, it is also indicated how many stars that were integrated have the same resonance of the star (if applicable), with a superscript number to the left of the stream name, the number indicating how many stars are on the same resonance. For two streams, there were no candidate members with distances nor radial velocity data available (Jet and Palomar 13). These streams are also not investigated further, since they are not on a resonant orbit.

4.1 Resonant orbits according to frequency analysis

As can be seen in table 1, there are six streams (300S, C-12, C-13, Elqui, NGC 1851, NGC 7492) that are determined to be resonant using frequency analysis. In the following, we will go into more depth into those six streams. We will show the orbits, and where possible, we compare them to integrations of candidate members belonging to the respective streams. All orbits of stream candidates for which the stream was determined to be on a resonance using frequency analysis can be found in the Appendix. We also show 5D projections of all streams determined to be on a resonance using frequency analysis below. 5D projections of all streams can be found in Appendix as well.

4.1.1 300S

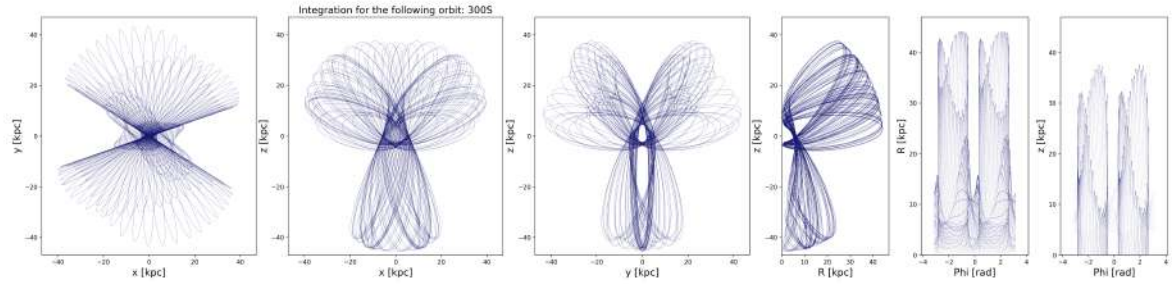

Figure 7: Integrated orbit of 300S, in both Cartesian and Cylindrical coordinates

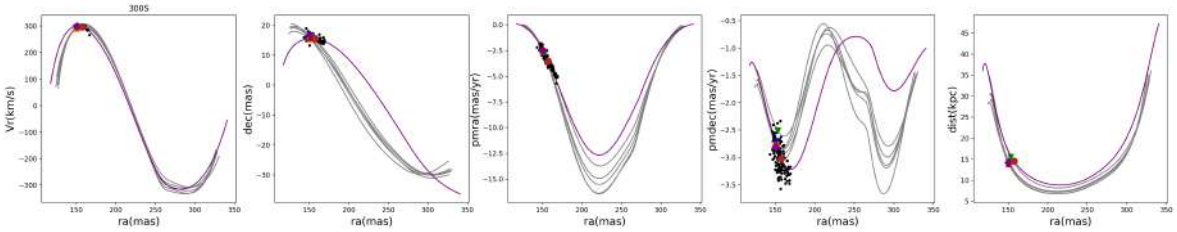

Figure 8: Right Ascension vs all other ICRS coordinates for the stream 300S

In figure 7, the orbit of 300S is shown. According to frequency analysis, the stream has a resonance $\Omega_R : \Omega_Z : \Omega_\phi = 3 : 2 : 2$ up to 10^{-3} and a resonance $\Omega_Z : \Omega_\phi = 1 : 1$ with a tolerance up to 10^{-4}. With visual inspection, we would classify this as a resonant orbit. We can see this by

Stream name	Lyap. exp.	T=10^{-3}	T=10^{-4}	Visual
[0]300S	0.0	$\Omega_R : \Omega_Z : \Omega_\phi = 3:2:2$	$\Omega_Z : \Omega_\phi = 1:1$	✓
ATLAS-Aliqa Uma	0.0	-	-	✓
[0]C-12	0.0	$\Omega_Z : \Omega_\phi = 1:1$	-	×
[0]C-13	0.0	$\Omega_Z : \Omega_\phi = 1:1$	$\Omega_Z : \Omega_\phi = 1:1$	✓
C-19	0.0	-	-	✓
C-20	0.0	-	-	✓
C-24	0.0	-	-	✓
C-25	0.0	-	-	✓
[1]Elqui	0.0	$\Omega_R : \Omega_Z : \Omega_\phi = 3:2:2$	-	✓
Gaia-12	0.0	-	-	✓
Jet	0.0	-	-	✓
NGC 1261	0.2747	-	-	✓
[2]NGC 1851	0.2787	$\Omega_Z : \Omega_\phi = 1:1$	$\Omega_Z : \Omega_\phi = 1:1$	×
NGC 2298	0.0231	-	-	✓
NGC 5466	0.0	-	-	✓
[5]NGC 7492	0.0	$\Omega_Z : \Omega_\phi = 1:1$	$\Omega_Z : \Omega_\phi = 1:1$	✓
New-1	0.0	-	-	✓
New-4	0.0	-	-	✓
Orphan-Chenab	0.0	-	-	✓
Palomar 13	0.0	-	-	✓
Palomar 5	0.0	-	-	✓
Phoenix	0.0	-	-	✓
Sagittarius	0.0	-	-	✓
Spectre	0.0	-	-	✓
Tucana III	0.1735	-	-	✓

Table 1: Streams with their respective resonances found using frequency analysis and checked by visual inspection, for decreasing tolerances. Column 1: Name of stream for which the resonances were determined. Column 2: Lyapunov exponent, see section 1 for more information. Column 3 and 4: Resonances for decreasing tolerances determined using frequency analysis described in 3.2. Column 5: Checks if the plots of the streams agree with the corresponding resonances by visually inspecting them.

looking at the second and third plot from the left; the orbit is asymmetric when we mirror in the z-plane. There are, however, some things to say about the resonances in the other coordinates. Since the orbit does not come back to the same point after one cycle and it is not an a super thin line, this means that the orbit is not exactly on the resonance, but librating slightly around it.

In figure 8 it can be seen that in RA vs DEC and RA vs PMDEC, the orbit of the candidate members deviate from the orbit of the stream. We also did frequency analysis for these orbits, and none of them are resonant. In fact, all of the candidate members are following a chaotic orbit according to our frequency analysis. An example of this can be found in figure 9. The orbit of the candidate member also has a smaller apocenter, indicating that it is probably not a member.

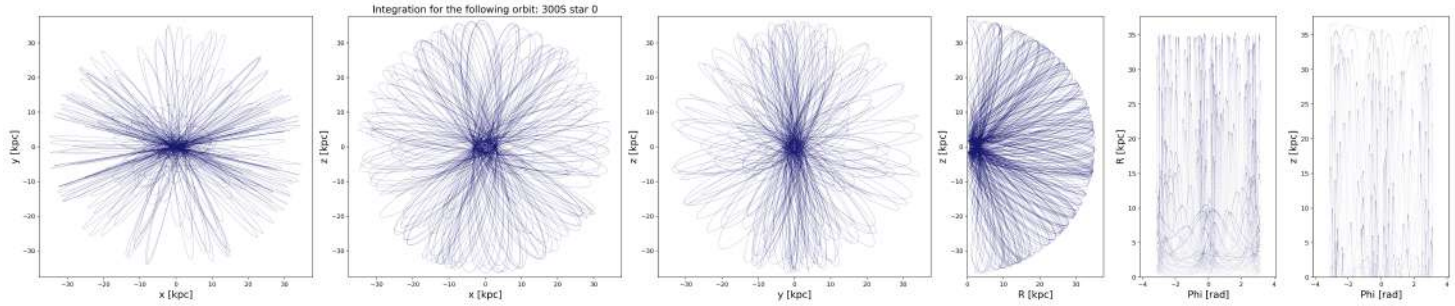

Figure 9: Integration of 300S for star 0

4.1.2 C-12

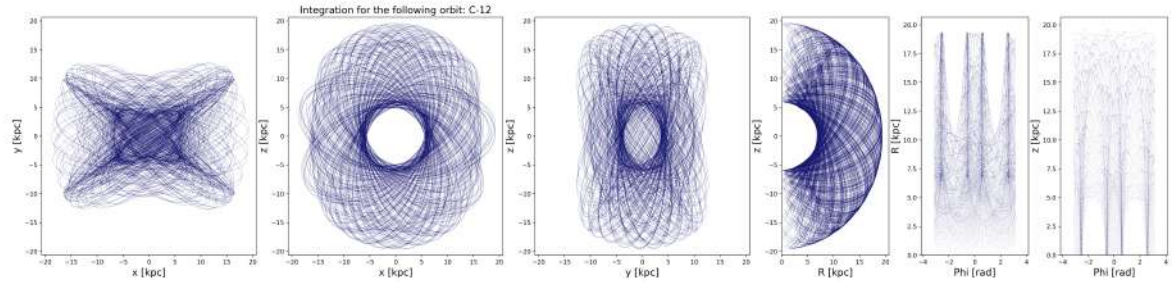

Figure 10: Integrated orbit of C-12, in both Cartesian and Cylindrical coordinates

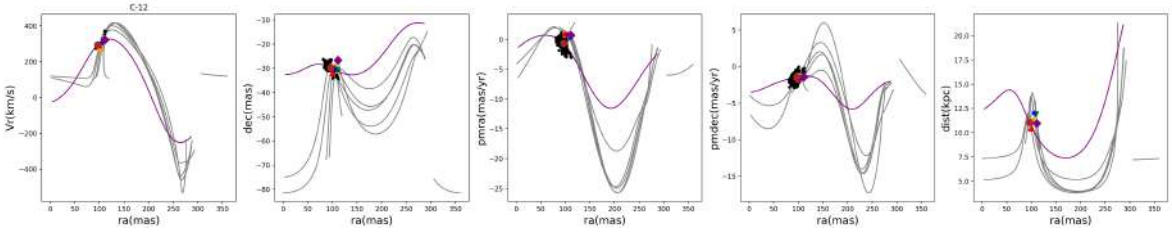

Figure 11: Right Ascension vs all other ICRS coordinates for the stream C-12

In figure 10, the orbit of C-12 is shown. According to frequency analysis, the stream has a resonance $\Omega_Z : \Omega_\phi = 1 : 1$ with a tolerance up to 10^{-3}. With visual inspection, we however do not see direct signs of this being a resonant orbit. This likely means that the tolerance is too large for this specific resonance.

Another thing to note about this stream, is that the candidate members are somewhat different (see figure 11) from the orbit obtained from the integration of the initial conditions of

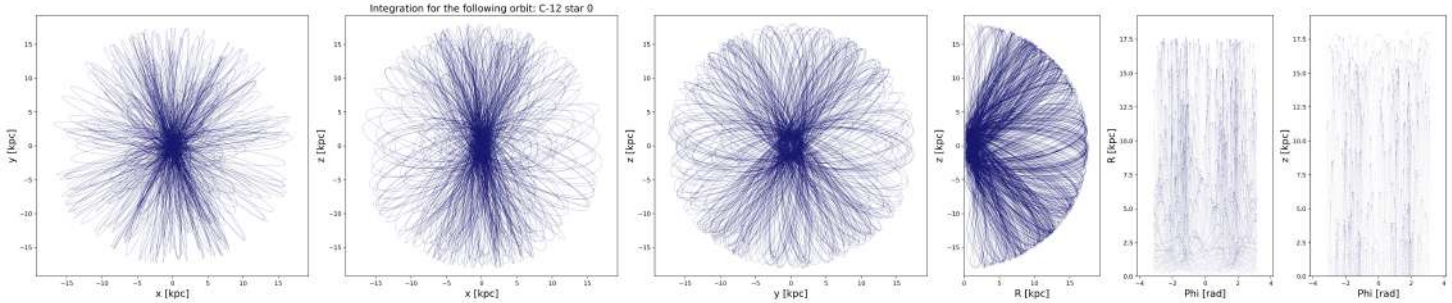

Figure 12: Integration of C-12 for star 0

the stream, as given by Bonaca & Price-Whelan (2024). The orbits of these members are also all chaotic, as they have a Lyapunov exponent >0. One of these orbits can be found in figure 12. This orbit has a smaller apocenter than the orbit of the stream's initial conditions as well, indicating some discrepancies.

4.1.3 C-13

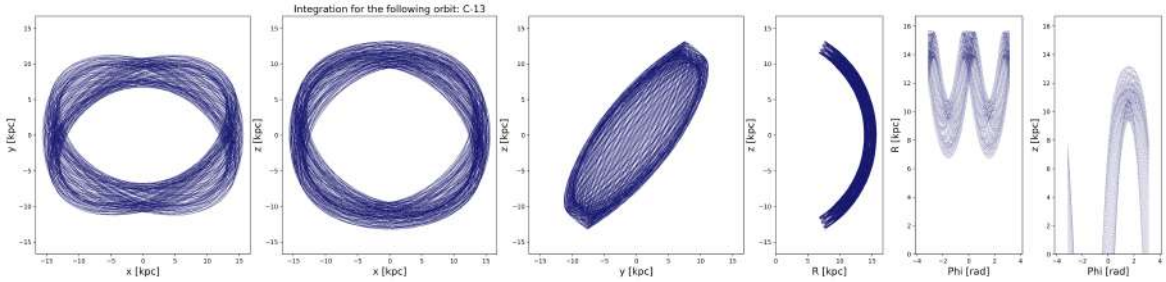

Figure 13: Integrated orbit of C-13, in both Cartesian and Cylindrical coordinates

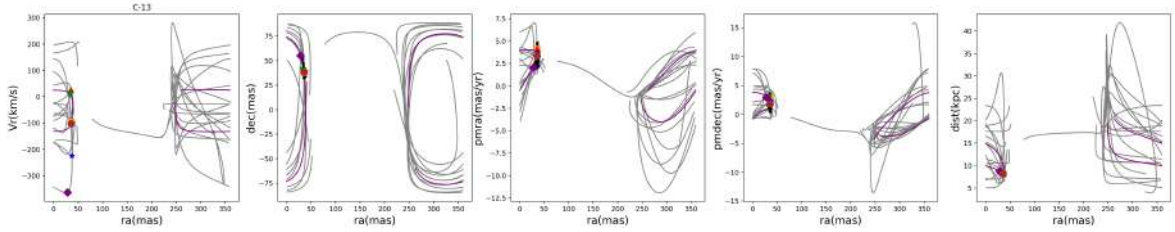

Figure 14: Right Ascension vs all other ICRS coordinates for the stream C-13

In figure 13, the orbit of C-13 is shown. According to frequency analysis, the stream has a resonance $\Omega_Z : \Omega_\phi = 1 : 1$ with a tolerance up to 10^{-4}. Using visual inspection, we would classify this as a resonant orbit; in figure 13 in the third plot from the left, we can see that it is asymmetric when we flip axes. This can indicate a resonant orbit, as mentioned in section 3.3. It is also a bit flattened in the y-z plane, indicative of resonances.

We also note in figure 14 that one of the stars is deviating more from the stream's orbit than the other stars. This is probably because we selected an outlier. We integrated the orbits of the stream candidates, and the outlier seems to indeed have a slightly different orbit, though this

is a very tentative statement. All stream candidates have regular orbits according to frequency analysis, though the outlier seems to have some resonance in R and Z, as it closely follows its previous loops. Figure 15 is a one of these candidate members, whereas figure 16 is the outlier.

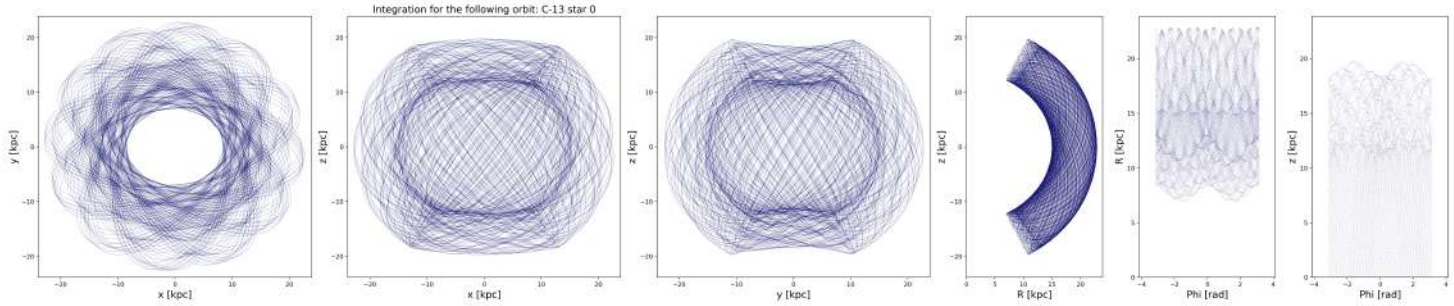

Figure 15: Integration of C-13 for star 0

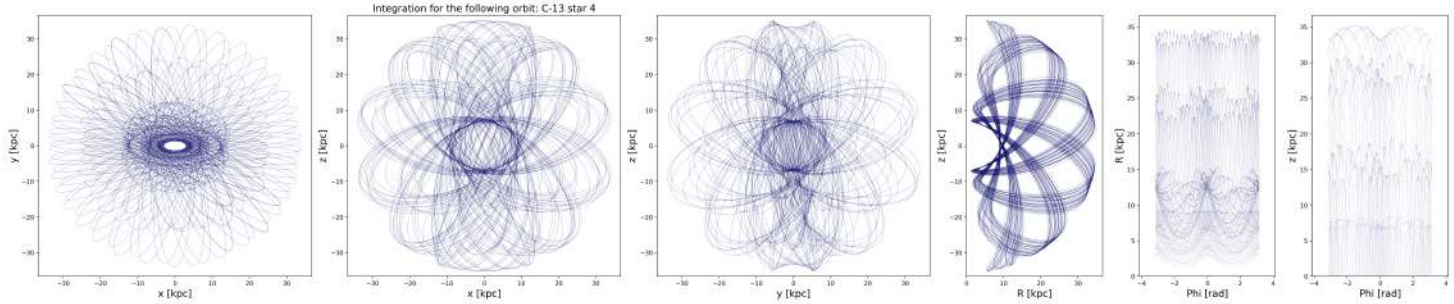

Figure 16: Integration of C-13 for star 4

4.1.4 Elqui

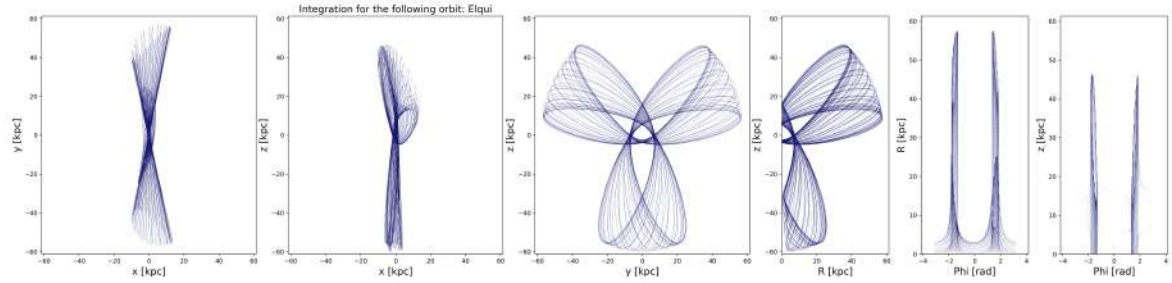

Figure 17: Integrated orbit of Elqui, in both Cartesian and Cylindrical coordinates

In figure 17, the orbit of Elqui is shown. According to frequency analysis, the stream has a resonance $\Omega_R : \Omega_Z : \Omega_\phi = 3 : 2 : 2$ with a tolerance up to 10^{-3}. By visual inspection, the orbit also seems to be resonant in all three cylindrical coordinates; it comes back to approximately the same point after one orbit. Another way that we can see that it is resonant is by looking at the second and third plot from the left. When we mirror the orbit in the z-axis, we can see that it is asymmetric, implying resonance. Furthermore, it occupies a pretty thin plane, which is indicative of a resonance.

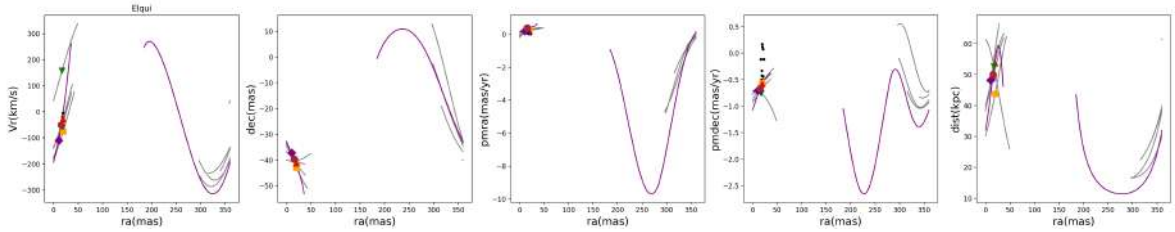

Figure 18: Right Ascension vs all other ICRS coordinates for the stream Elqui

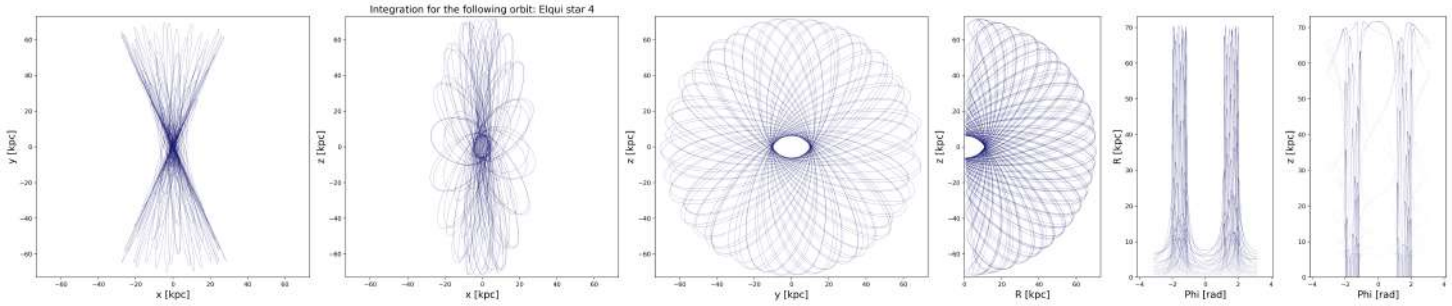

Figure 19: Integration of Elqui for star 4

Figure 18 shows that the orbits of the candidate members follow the orbit of the stream. The integrated orbits of the candidate members also look similar in the fact that it looks like the plane is flattened. An example of one of these can be found in figure 19, which is also the only star that has a similar resonance as the stream: $\Omega_Z : \Omega_\phi = 1 : 1$. The candidate members might be a bit farther away from the resonance, as they occupy more space.

4.1.5 NGC 1851

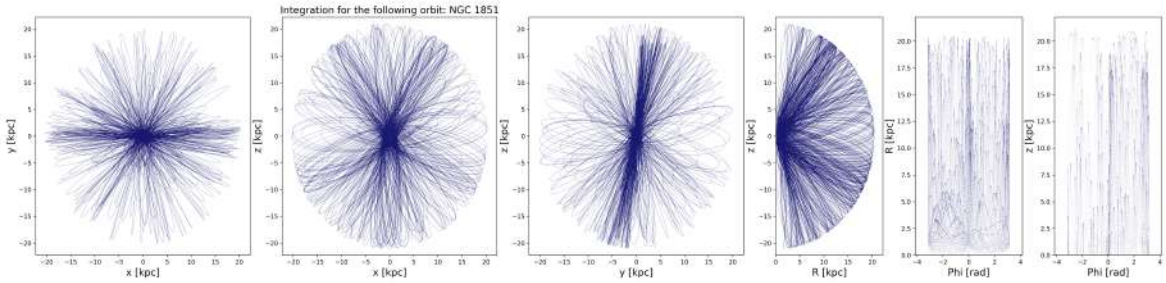

Figure 20: Integrated orbit of NGC 1851, in both Cartesian and Cylindrical coordinates

In figure 20, the orbit of NGC 1851 is shown. According to frequency analysis, the stream has a resonance $\Omega_Z : \Omega_\phi = 1 : 1$ with a tolerance up to 10^{-4}. By visual inspection, we would not classify the orbit as strictly resonant. However, it does kind of occupy limited space in the yz plane. This can be seen by that fact that there is a flattened overdensity. This could indicate the orbit was close to a resonance over a short period of time. In table 1, under the second column, it says that this orbit has a Lyapunov exponent of 0.2787, indicating a mildly chaotic orbit. This means we can rely less on the resonance determined by frequency analysis. Together with the fact that it visually does not seem resonant, this orbit is most likely not truly on a resonant

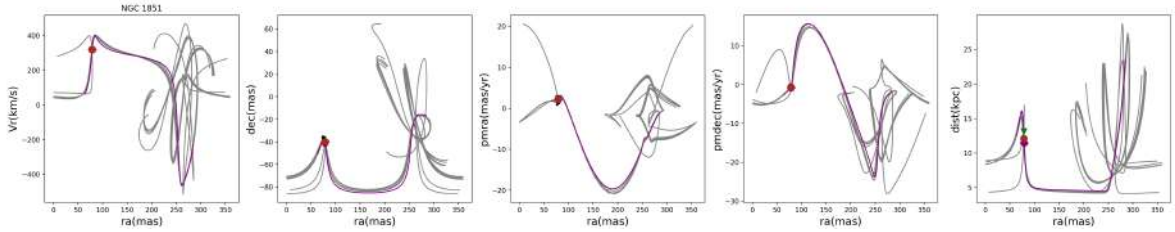

Figure 21: Right Ascension vs all other ICRS coordinates for the stream NGC 1851

orbit. To see where the apparent resonance determined by frequency analysis comes from, we integrated this stream's initial condition for 100 Gyr and split the orbit up into 5 segments: 0-20 Gyr, 20-40 Gyr, 40-60 Gyr, 60-80 Gyr and 80-100 Gyr (we call them segment 1, 2, 3, 4 and 5 respectively). We then plot all of those segments to visually inspect if it is resonant over some time. These plots can be found in figure 22. For the y vs z panel (third row), it can be seen that the orbit is close to a resonance for segment 2 and 3 (mostly for segment 3). We can see this because if you mirror in the z-axis, there is an asymmetry. We can also vaguely see it in the ϕ vs R panel (row 5); the cycles of orbits are centering around $\phi = 0$. These could be arguments for why a resonance was found using frequency analysis.

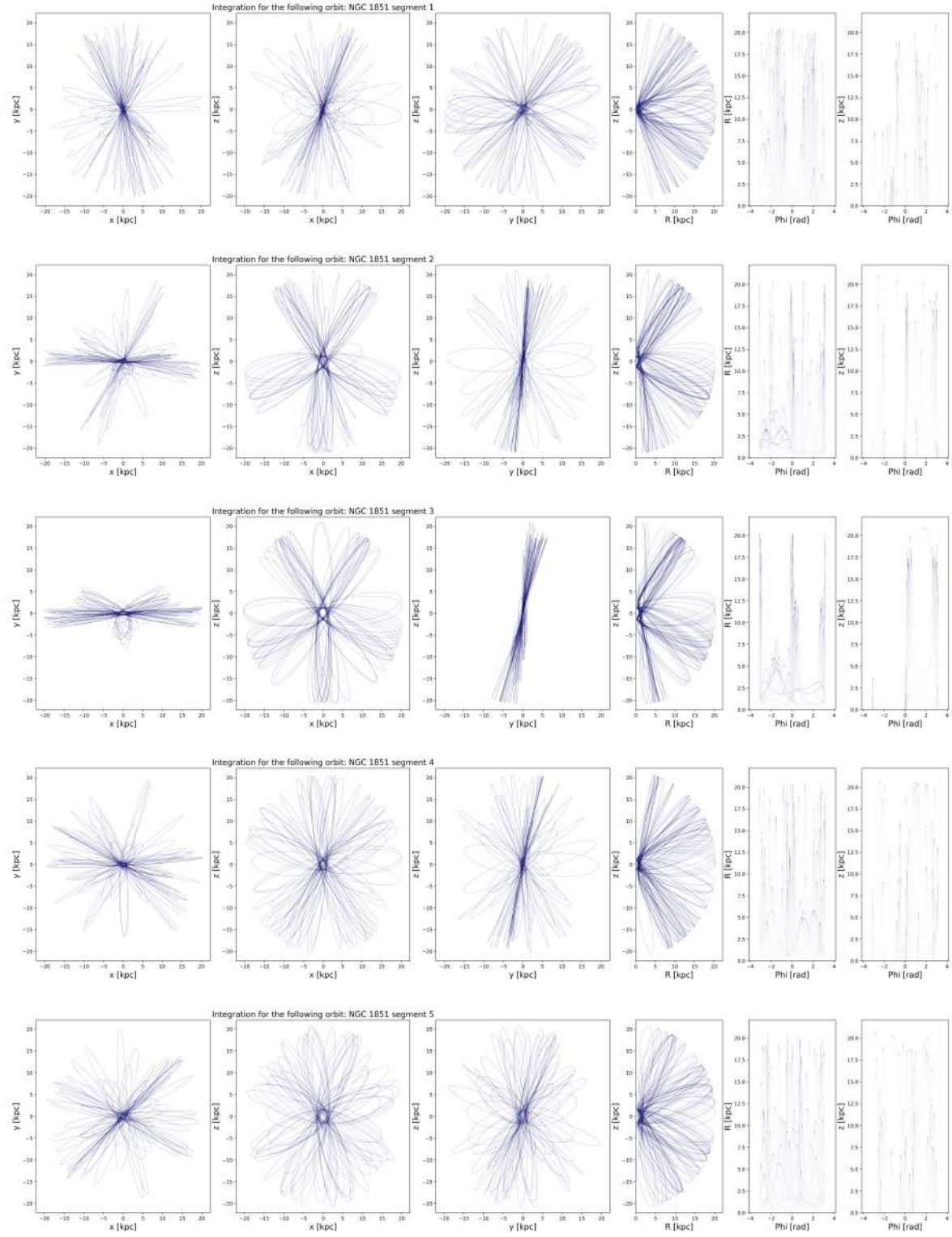

Figure 22: Segment plots of NGC 1851

4.1.6 NGC 7492

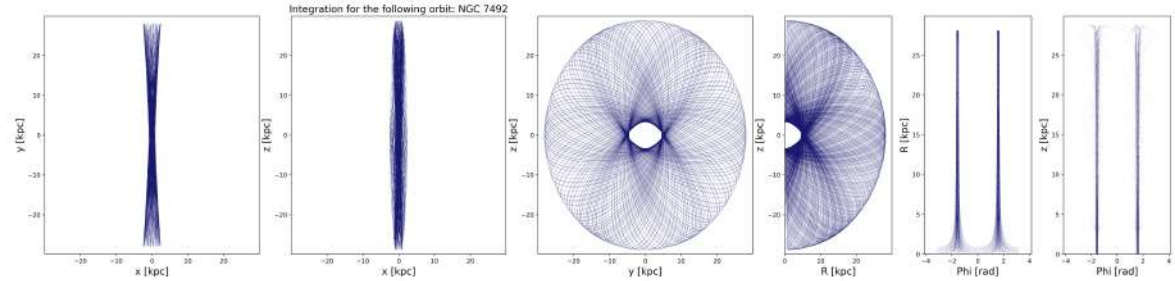

Figure 23: Integrated orbit of NGC 7492, in both Cartesian and Cylindrical coordinates

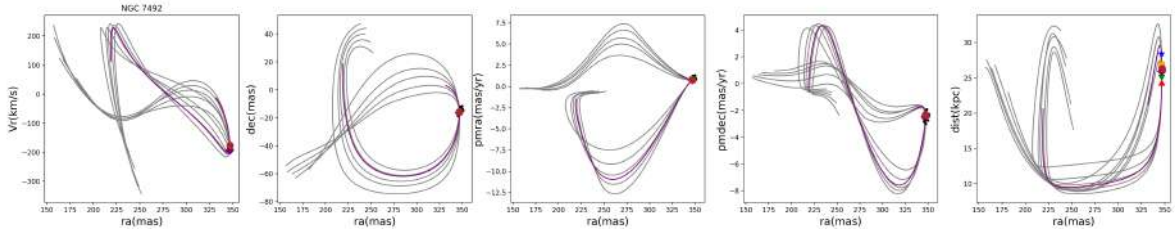

Figure 24: Right Ascension vs all other ICRS coordinates for the stream NGC 7492

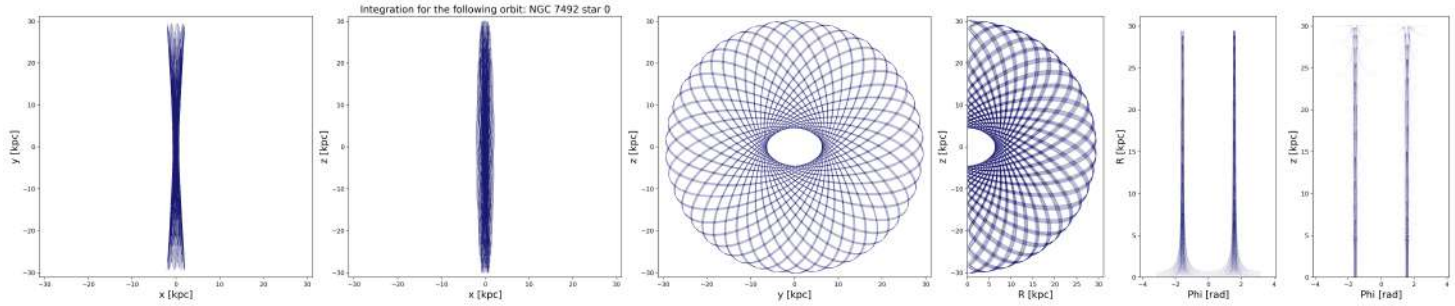

Figure 25: Orbit of a candidate member of NGC 7492, that we call star 0.

In figure 23, the orbit of NGC 7492 is shown. According to frequency analysis, the stream has a resonance $\Omega_Z : \Omega_\phi = 1 : 1$ with a tolerance up to 10^{-4}. By visual inspection, the orbit also seems to be resonant in these coordinates (column 5 in figure 23), since there is a large portion of space that is not occupied by the orbit, and the space that it occupies are very narrow lines. Additionally, the orbit seems to be resonant in R and Z by visual inspection for the same reason, but according to frequency analysis this is not the case. A speculative reason for this could be that they are on a higher-order resonance, which we do not take into account in our analysis.

All candidate members for this stream that we integrated are also on the same resonance as the stream. One of these orbits can be found in figure 25. Additionally, the stars' orbits closely match that of the stream (see figure 24).

4.1.7 Non-resonant orbits

We also did a brief visual inspection for the orbits for which no resonances were found using frequency analysis. The frequency analysis seems to be done correctly for those, since they also don't seem resonant by visual inspection. Two examples of this can be found in figure 26, which are the orbits of Sagittarius and ATLAS-Aliqa Uma.

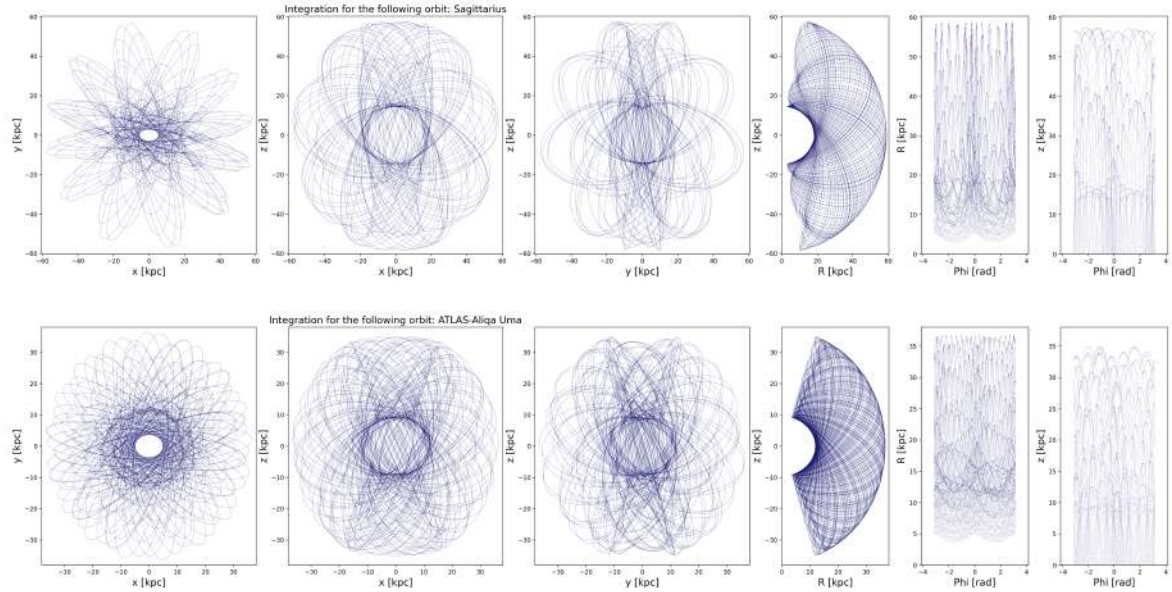

Figure 26: Integrated orbit of Sagittarius and ATLAS-Aliqa Uma, in both Cartesian and Cylindrical coordinates

5 Discussion

4 of the 25 streams that we analyzed are are very close to being on a resonant orbit, as the ratio of two of their orbital frequencies differs from a ratio of integers by less than 10^{-3}. For only one of the streams (NGC 7492), all the candidate members that we integrated are on the same resonances, both by frequency analysis and by visual inspection. The candidate members that we integrated also seem to be on a similar orbit as the stream. Therefore, for this stream the orbit is fully inside the resonant region.

Two of the streams that are on a resonance according to frequency analysis have at least one candidate member that is also on the same resonance. These streams are Elqui and NGC 1851.

For Elqui, the stream is doubly resonant, with a frequency ratio of $\Omega_R : \Omega_Z : \Omega_\phi = 3 : 2 : 2$. This can be reasoned with the fact that there is an asymmetry in some of the planes. One of the candidate members is also on a similar resonance, though it is singly resonant rather than doubly resonant. Judging from figure 18, the integrated orbits of the tentative members seem to be following the orbit of the star. Comparing the orbits of the stream in Galactocentric Cartesian coordinates to the orbits of the candidate members, we see that the orbits are also slightly similar (see figure 17 and 19). They have similar apocenters, and the space they occupy in the xy and xz plane is also similar.

For NGC 1851, the stream is on a resonance according to frequency analysis. However, it also has a Lyapunov exponent >0, implying it is on a chaotic orbit. However, an orbit cannot be resonant and chaotic at the same time. This means that we can rely less on the frequency analysis. The orbit of the stream did seem to be close to a resonance over a certain amount of time, when we plotted the segments. We also integrated candidate members, and two of these are determined to be on the same resonance, though they are determined to be doubly resonant (8:5:5). These resonances can also be seen in the plots, but the orbit is also not strictly following the resonance, most likely due to the fact that it has a Lyapunov exponent >0, implying that it is chaotic, and thus it cannot be strictly on a resonance. All of the other candidate members are also chaotic, so the stream and its stars are most likely truly on a chaotic orbit.

Three of the streams that are on a resonance have no candidate members on a resonance. These are C-12, C-13 and 300S. The candidate members of these streams are also not closely following the orbits shown in the projections in all six ICRS coordinates. Notably, the stream candidates themselves are all on very similar orbits, which are different from the stream's initial condition. This might suggest that the stream's initial condition is off. A reason that the orbit possibly does not match the stream, is because at pericenter, the orbit delineates the stream, but at apocenter, it is misaligned with the stream's candidate members Bonaca & Price-Whelan (2024). This means that it is not always appropriate to represent a stream as on orbit (Eyre & Binney (2009), Eyre & Binney (2011), Sanders & Binney (2013a), Sanders & Binney (2013b)).

The candidate members of 300S and C-12 are all following a chaotic orbit, whereas the candidate members of C-13 are all following a regular orbit. Since the candidate members do not match the stream's orbit, we cannot safely say if the stream is truly on a resonance, and the found resonances are inconclusive.

5.1 Limitations

The work of Woudenberg & Helmi (2024), which is the potential we used in this thesis, made a few simplifying assumptions. First of all, it assumed a NFW profile, for which the axes are aligned with the disk of the Milky Way. However, some more recent work suggested that the Milky Way halo may be tilted (Han et al. (2023b), Han et al. (2023a)), contracted (e.g. Cautun et al. (2020)), and the shape of its mass distribution may vary with radius (e.g. Cataldi et al.

(2023)). Moreover, a static potential is assumed. However, the Large Magellanic Cloud is also thought to affect the dynamics of the potential (Woudenberg & Helmi (2024)). In fact, it has been shown to affect the stream Orphan-Chenab (e.g. Lilleengen et al. (2023)). For a more realistic model of the potential, it might also be interesting to take into account other the LMC. In recent work, Woudenberg & Helmi (2025) showed that the Galactic bar also influences dynamics of stars, which also has not been taken into account. Though we are probing streams that are sufficiently far away from the Milky Way bar today, some come close enough to the bar to sufficiently perturbate the orbit of the stream. It would be interesting to further investigate this, but due to time constraints, it was not possible for us to do this. Furthermore, the potential is constrained within 20 kpc, meaning the results found for streams that are further away than this today should be taken with caution.

A part of our analysis was done using visual inspection. This is a very tentative and speculative way of analyzing streams. To get more robust results, it would be good if a more analytical method is used to judge whether the candidate members are on the same orbit.

We were also limited by the fact that most of the stellar data we used does not have measured distance data (only candidate members for Sagittarius do), which caused the distance we assigned to the stars to be a free parameter. We had to sample within a 5% error of the inferred distance of the stream. This means that the actual distance of the candidate members may not at all match the distance we assigned to them, possibly causing the results of the candidate members to be less accurate. Next to that, some candidate members did not have radial velocity data, meaning that some of the streams had less than 5 candidate members. For those streams, we sampled within the error of one of the measured data points.

5.2 Other considerations

We also considered to use data from the `galstreams` library[2], but these initial conditions are less reliable. This data is made up of tracks that are obtained through empirical fits to observed data (Mateu (2023)), rather than orbital fits as for data from Bonaca & Price-Whelan (2024) . This paper also advises user discretion, since for some tracks the stellar proper motion and radial velocity is predicted based on a model that is not checked for confidence and robustness of the detection. Hence, we chose to use the `streams_overview` library Bonaca & Price-Whelan (2024), which is based on a physical model.

5.3 Additional findings

5.3.1 Stream alignment of candidate members

As we saw in section 4.1, most of the stream's orbit align with the stream's candidate members. There does not seem to be a correlation between the Galactocentric distance today and whether the orbits of candidate members fit the stream. This might indicate that Milky Way potential we used might be close to reality for distances > 20 kpc as well. Due to time constraints, we could not investigate this further, but it would be interesting to do so in the future.

As was already mentioned in section 4.1, a few candidate members do not align with the orbit of their stream. We list all the streams that consistently do not match with their candidate members, meaning it is not just one outlier not matching with the stream. We do this based on visual inspection: 300S, C-12, Orphan-Chenab, Palomar 5.

[2]https://github.com/cmateu/galstreams

5.3.2 Metallicity spread of Elqui

For one of the streams without a known progenitor (Bonaca & Price-Whelan (2024)), we plotted the metallicity spread of the candidate members with measured metallicity data in figure 27 to see what their possible progenitor could be. This was the only stream on a resonance according to frequency analysis with metallicity data. Globular clusters are mono-metallic, whereas (dwarf) galaxies have a spread in metallicities (Beasley (2020)). Within the errors seen in figure 27, it could be argued that some of the tentative members with measurements are approximately mono-metallic, but if we just look at the data points, they are not and it could be argued that they are a dwarf galaxy. Thus the results of the metallicity spread of Elqui are inconclusive.

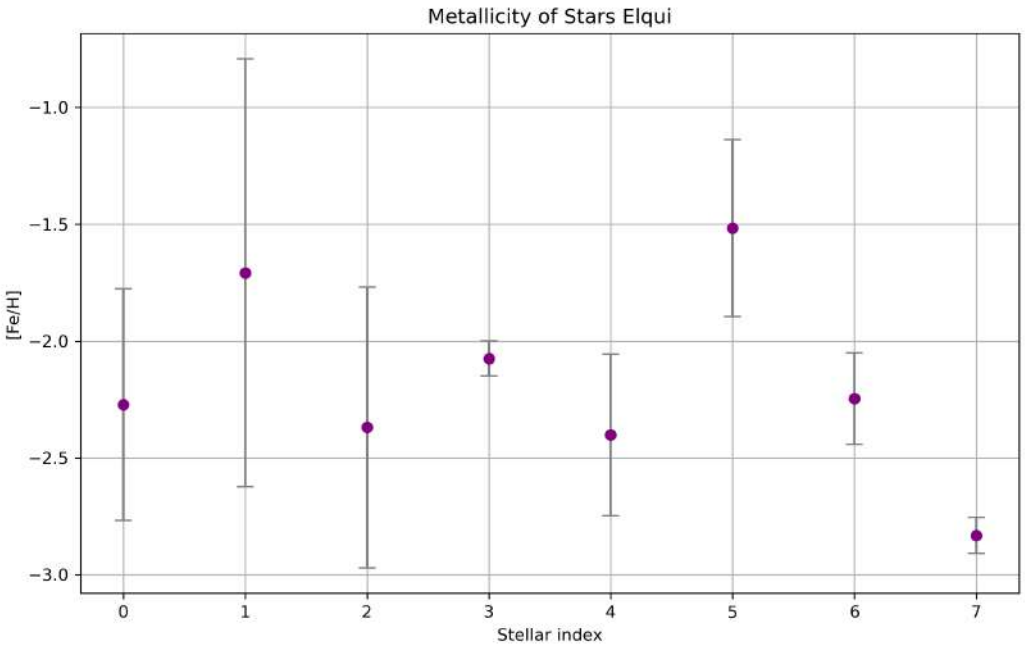

Figure 27: Metallicities of candidate members for Elqui.

6 Conclusions

In this thesis we analyzed 25 streams whether they are on a resonances. We used initial conditions of streams that were inferred from stellar data and selected the streams which are on a Galactocentric distance >15 kpc today. We integrated the streams in the potential from Woudenberg & Helmi (2024) and determined their frequencies using `SuperFreq`. Using these frequencies, we determined the lower-order resonances of the streams. Additionally, we integrated the orbits of candidate members of each stream to assess whether they are on a similar orbit and/or resonance. For one of the resonant streams, we also assessed the metallicity of Elqui to assess what a possible progenitor of the stream could be. Our conclusions are as follows:

- 6 of the 25 streams are determined to be on resonant orbits using frequency analysis. These streams are 300S, C-12, C-13, Elqui, NGC 1851 and NGC 7492. For one of these streams (NGC 7492), all candidate members in our subset are on the same resonance, and by visual inspection on the same orbit. For two of the streams (Elqui and NGC 1851), at least one candidate member of our subset is on the same resonance using frequency analysis. NGC 1851 is on a chaotic orbit, including its candidate members of our subset. For the remaining streams, no candidate members of our subsets are on the same resonance. These streams also don't seem to match the orbit based on visual inspection. All candidate members of our subset of C-12 and 300S are on a chaotic orbit and all candidate members of our subset of C-13 are on a regular orbit. So out of the 25 streams, we find that 4 are on a resonant orbit by both visual inspection and frequency analysis.
- The metallicities of the candidate members of Elqui do not provide us with sufficient information as to whether the progenitor of the stream is a globular cluster or a dwarf galaxy.
- Four of our assessed streams (NGC 1261, NGC 1851, NGC 2298, Tucana III) have Lyapunov exponents higher than 0, indicating they are on a chaotic orbit.
- Most orbits of the stream's initial conditions matched the orbit of our subset of candidate members, suggesting the Milky Way halo potential we used is close to reality. For 4 out of 25 streams, orbits of our subset of candidate members do not match the orbit of the stream's initial conditions (300S, C-12, Orphan-Chenab, Palomar 5).

For future work, we suggest the stream's orbits are integrated in a more complex and realistic potential. When more data is released (e.g. Gaia DR4, Gaia DR5), we suggest integrating candidate members with new data, possibly with distance data, for more reliable results. We also suggest a more robust method is used for judging whether a stream follows the same orbit as its candidate members.

References

Abuter R., et al., 2018, Astronomy & Astrophysics, 615, L15

Awad P., et al., 2024, Astronomy & Astrophysics, 683, A14

Beasley M. A., 2020, Reviews in Frontiers of Modern Astrophysics: From Space Debris to Cosmology, pp 245–277

Bonaca A., Price-Whelan A. M., 2024, New Astronomy Reviews, p. 101713

Bonaca A., Hogg D. W., Price-Whelan A. M., Conroy C., 2019, The Astrophysical Journal, 880, 38

Bonaca A., et al., 2020, The Astrophysical Journal Letters, 892, L37

Borsato N. W., Martell S. L., Simpson J. D., 2020, Monthly Notices of the Royal Astronomical Society, 492, 1370

Bovy J., 2016, Physical review letters, 116, 121301

Bovy J., Bahmanyar A., Fritz T. K., Kallivayalil N., 2016, The Astrophysical Journal, 833, 31

Cataldi P., et al., 2023, Monthly Notices of the Royal Astronomical Society, 523, 1919

Cautun M., et al., 2020, Monthly Notices of the Royal Astronomical Society, 494, 4291

Chandra V., et al., 2022, The Astrophysical Journal, 940, 127

Dodd E., Helmi A., Koppelman H. H., 2022, Astronomy & Astrophysics, 659, A61

Eilers A.-C., Hogg D. W., Rix H.-W., Ness M. K., 2019, The Astrophysical Journal, 871, 120

Erkal D., Belokurov V., Bovy J., Sanders J. L., 2016, Monthly Notices of the Royal Astronomical Society, 463, 102

Eyre A., Binney J., 2009, Monthly Notices of the Royal Astronomical Society, 400, 548

Eyre A., Binney J., 2011, Monthly Notices of the Royal Astronomical Society, 413, 1852

Ferguson P., et al., 2021, The Astronomical Journal, 163, 18

Gaia Collaboration G., et al., 2017, A&A, p. A19

Gaia Collaboration et al., 2018, Astronomy & Astrophysics, 616, 1

Gaia Collaboration G., et al., 2023, astrophysics, 674, A41

Gatto M., Napolitano N., Spiniello C., Longo G., Paolillo M., 2020, Astronomy & Astrophysics, 644, A134

Gibbons S., Belokurov V., Erkal D., Evans N., 2016, Monthly Notices of the Royal Astronomical Society: Letters, 458, L64

Grillmair C. J., 2019, arXiv preprint arXiv:1909.05927

Grillmair C. J., 2022, The Astrophysical Journal, 929, 89

Han J. J., Conroy C., Hernquist L., 2023a, Nature Astronomy, 7, 1481

Han J. J., Semenov V., Conroy C., Hernquist L., 2023b, The Astrophysical Journal Letters, 957, L24

Helmi A., Gomez F., 2007, arXiv preprint arXiv:0710.0514

Helmi A., White S. D., De Zeeuw P. T., Zhao H., 1999, Nature, 402, 53

Huang Y., Chen B.-Q., Zhang H.-W., Yuan H.-B., Xiang M.-S., Wang C., Tian Z.-J., Liu X.-W., 2019, The Astrophysical Journal, 877, 13

Ibata R. A., Gilmore G., Irwin M. J., 1995, Monthly Notices of the Royal Astronomical Society, 277, 781

Ibata R., et al., 2024, The Astrophysical Journal, 967, 89

Jurić M., et al., 2008, The Astrophysical Journal, 673, 864

Klypin A., Kravtsov A. V., Valenzuela O., Prada F., 1999, The Astrophysical Journal, 522, 82

Koposov S. E., et al., 2023, Monthly Notices of the Royal Astronomical Society, 521, 4936

Koppelman H. H., Helmi A., 2021, Astronomy & Astrophysics, 649, A55

Laskar J., 1993, Celestial Mechanics and Dynamical Astronomy, 56, 191

Li T. S., et al., 2021, The Astrophysical Journal, 911, 149

Lilleengen S., et al., 2023, Monthly Notices of the Royal Astronomical Society, 518, 774

Maffione N. P., Gómez F. A., Cincotta P. M., Giordano C. M., Cooper A. P., O'Shea B. W., 2015, Monthly Notices of the Royal Astronomical Society, 453, 2830

Malhan K., Ibata R. A., 2018, Monthly Notices of the Royal Astronomical Society, 477, 4063

Malhan K., Ibata R. A., 2019, Monthly Notices of the Royal Astronomical Society, 486, 2995

Mateu C., 2023, Monthly Notices of the Royal Astronomical Society, 520, 5225

McMillan P. J., 2017, Monthly Notices of the Royal Astronomical Society, 466, 174

Moore B., Ghigna S., Governato F., Lake G., Quinn T., Stadel J., Tozzi P., 1999, The Astrophysical Journal, 524, L19

Mróz P., et al., 2019, The Astrophysical Journal Letters, 870, L10

Necib L., Ostdiek B., Lisanti M., Cohen T., Freytsis M., Garrison-Kimmel S., 2020, The Astrophysical Journal, 903, 25

Odenkirchen M., et al., 2001, The Astrophysical Journal, 548, L165

Palau C. G., Miralda-Escudé J., 2023, Monthly Notices of the Royal Astronomical Society, 524, 2124

Papaphilippou Y., Laskar J., 1996, Astronomy and Astrophysics, v. 307, p. 427-449, 307, 427

Pettee M., Thanvantri S., Nachman B., Shih D., Buckley M. R., Collins J. H., 2024, Monthly Notices of the Royal Astronomical Society, 527, 8459

Posti L., Helmi A., 2019, Astronomy & Astrophysics, 621, A56

Price-Whelan A. M., 2015, Astrophysics Source Code Library, pp ascl–1511

Price-Whelan A. M., 2017, Journal of Open Source Software, 2, 388

Price-Whelan A. M., Johnston K. V., Valluri M., Pearson S., Küpper A. H., Hogg D. W., 2016, Monthly Notices of the Royal Astronomical Society, 455, 1079

Reid M. J., Brunthaler A., 2004, The Astrophysical Journal, 616, 872

Robitaille T. P., et al., 2013, Astronomy & Astrophysics, 558, A33

Sanders J. L., Binney J., 2013a, Monthly Notices of the Royal Astronomical Society, 433, 1813

Sanders J. L., Binney J., 2013b, Monthly Notices of the Royal Astronomical Society, 433, 1826

Shih D., Buckley M. R., Necib L., Tamanas J., 2022, Monthly Notices of the Royal Astronomical Society, 509, 5992

Shipp N., et al., 2019, The Astrophysical Journal, 885, 3

Shipp N., Price-Whelan A. M., Tavangar K., Mateu C., Drlica-Wagner A., 2020, The Astronomical Journal, 160, 244

Tian H.-J., et al., 2015, The Astrophysical Journal, 809, 145

Valluri M., Merritt D., 1998, The Astrophysical Journal, 506, 686

Vasiliev E., 2019, Monthly Notices of the Royal Astronomical Society, 482, 1525

Vasiliev B., 2021, J Phys Astron, 9, 238

Vasiliev E., Belokurov V., Erkal D., 2021, Monthly Notices of the Royal Astronomical Society, 501, 2279

Vera-Ciro C., Helmi A., 2013, The Astrophysical Journal Letters, 773, L4

Vogelsberger M., White S. D., Helmi A., Springel V., 2008, Monthly Notices of the Royal Astronomical Society, 385, 236

Woudenberg H. C., Helmi A., 2024, Astronomy & Astrophysics, 691, A277

Woudenberg H. C., Helmi A., 2025, arXiv preprint arXiv:2505.20143

Yang Y., Zhao J.-K., Ishigaki M. N., Chiba M., Yang C.-Q., Xue X.-X., Ye X.-H., Zhao G., 2022, Astronomy & Astrophysics, 667, A37

Yang Y., Zhao J.-K., Tang X.-Z., Ye X.-H., Zhao G., 2023, The Astrophysical Journal, 953, 130

Yoon J. H., Johnston K. V., Hogg D. W., 2011, The Astrophysical Journal, 731, 58

Zbinden O., Saha P., 2019, Research Notes of the AAS, 3, 73

e Silva L. B., Debattista V. P., Anderson S. R., Valluri M., Erwin P., Daniel K. J., Deg N., 2023, The Astrophysical Journal, 955, 38

A Appendix

Figure 28: 6D projection of all orbits.

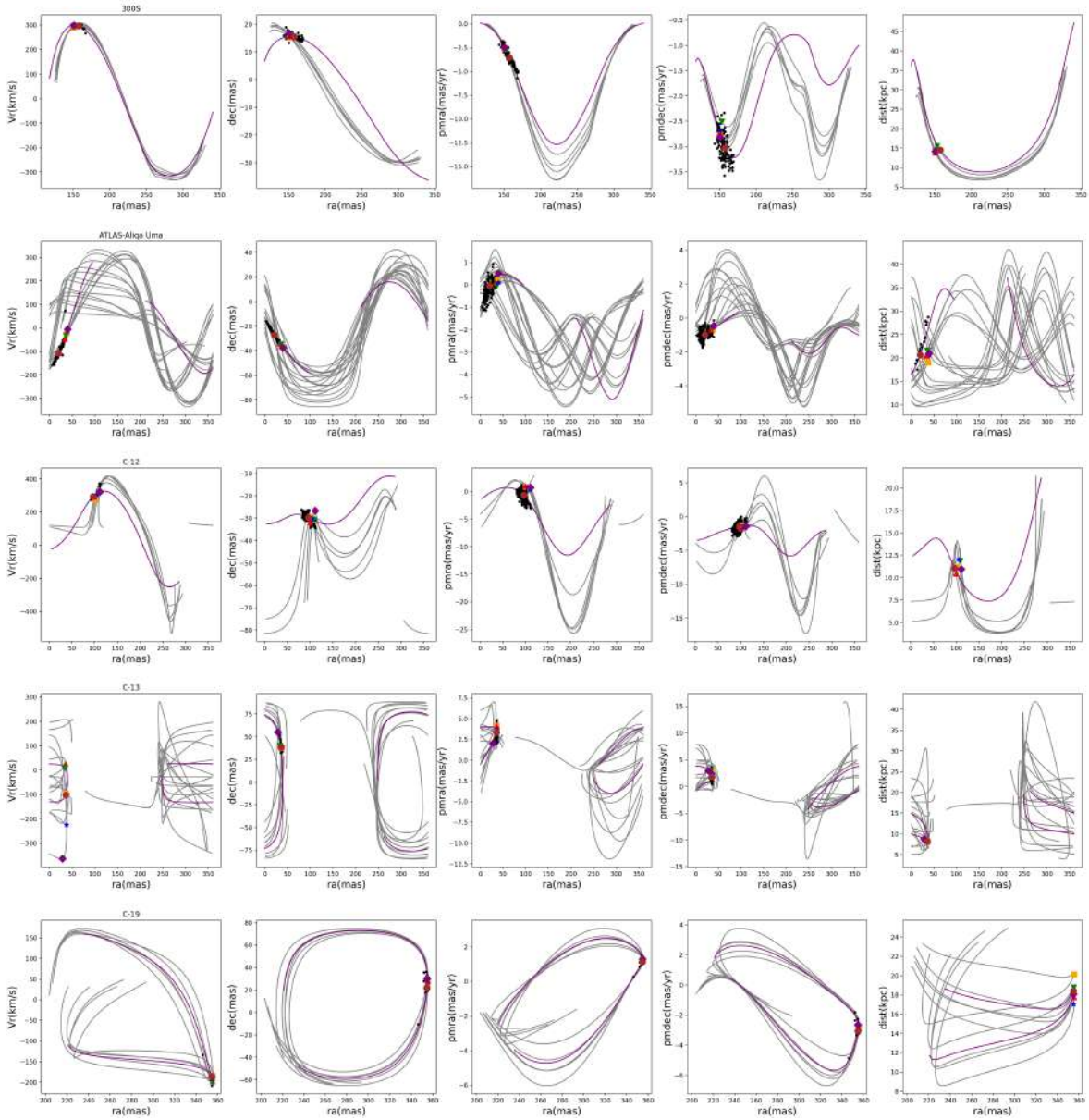

continued.

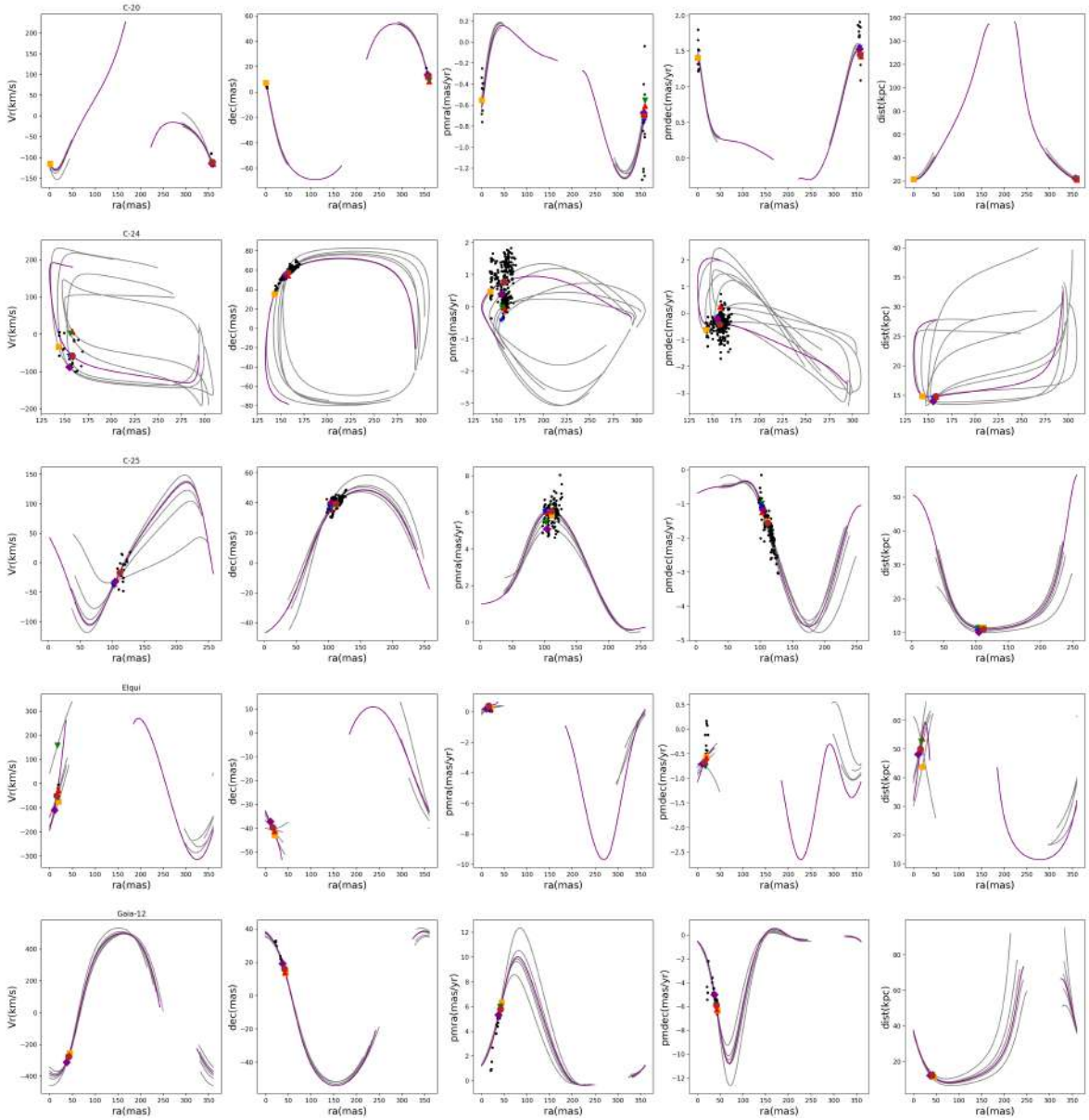
C-20
C-24
C-25
Elqui
Gaia-12
Vr(km/s)
dec(mas)
pmra(mas/yr)
pmdec(mas/yr)
dist(kpc)
ra(mas)

Figure 28: continued.

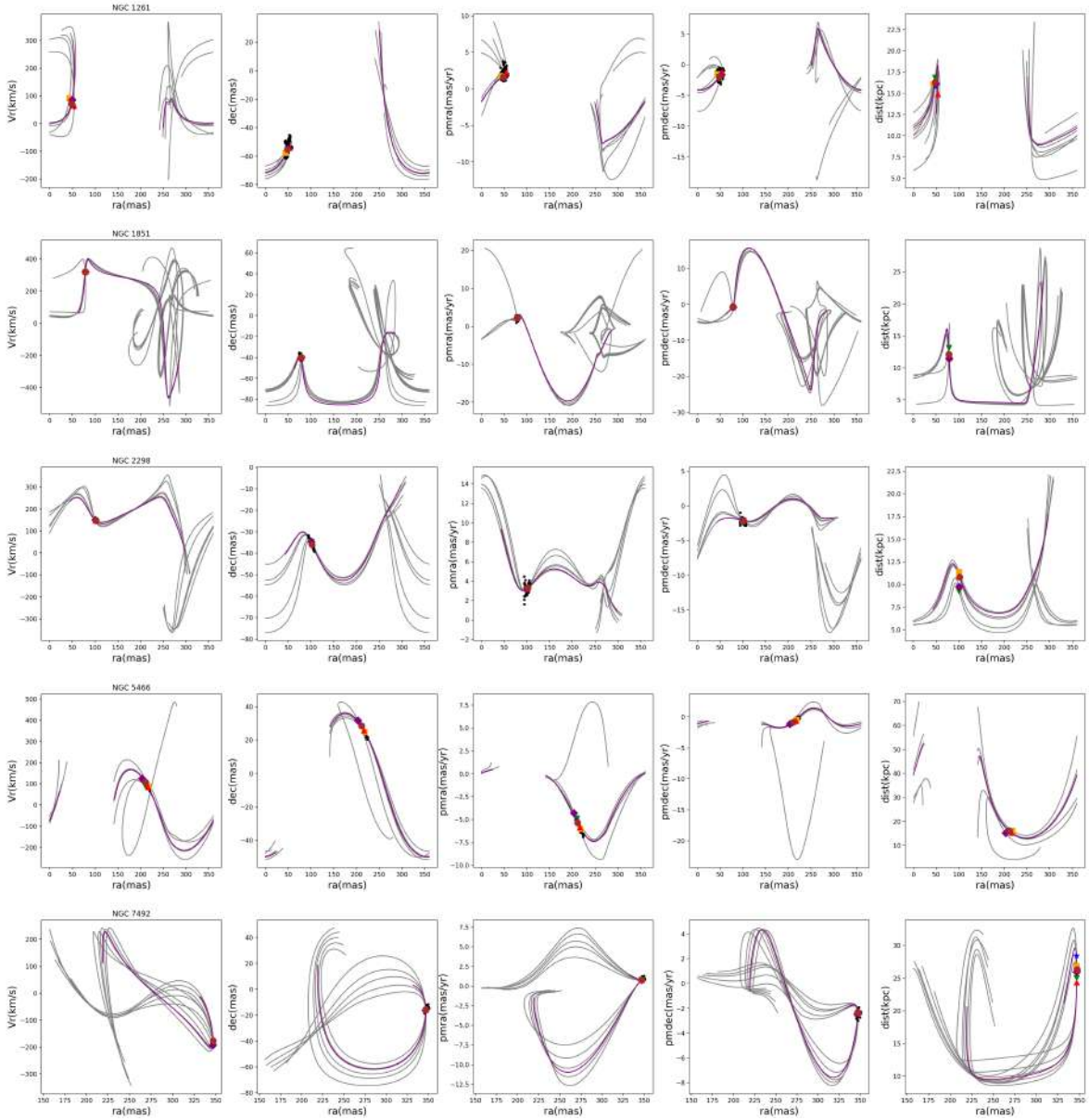

continued.

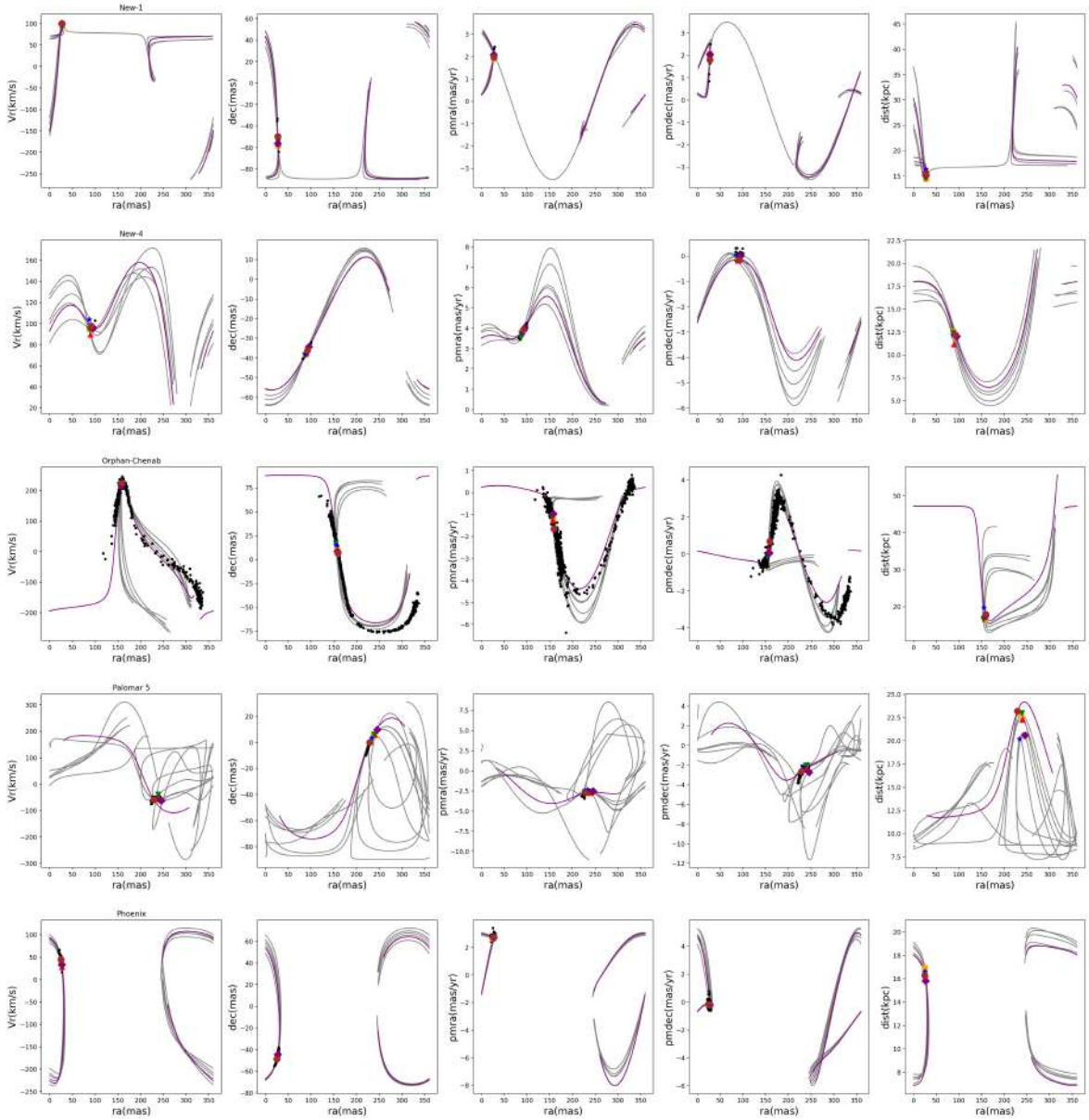
New-1
New-4
Orphan-Chenab
Palomar 5
Phoenix
Vr(km/s)
dec(mas)
pmra(mas/yr)
pmdec(mas/yr)
dist(kpc)
ra(mas)

continued.

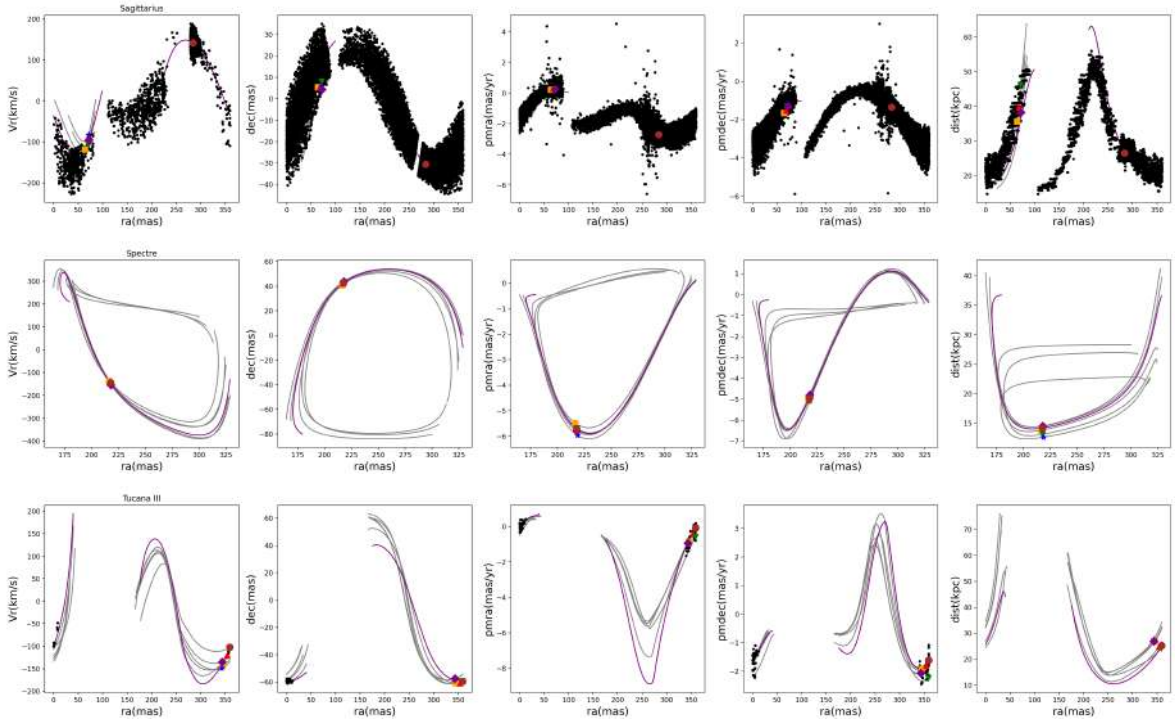
Sagittarius
Spectre
Tucana III
Vr(km/s)
dec(mas)
pmra(mas/yr)
pmdec(mas/yr)
dist(kpc)
ra(mas)

Figure 29: 6D projection of all orbits, zoomed in on the candidate members of the respective stream.

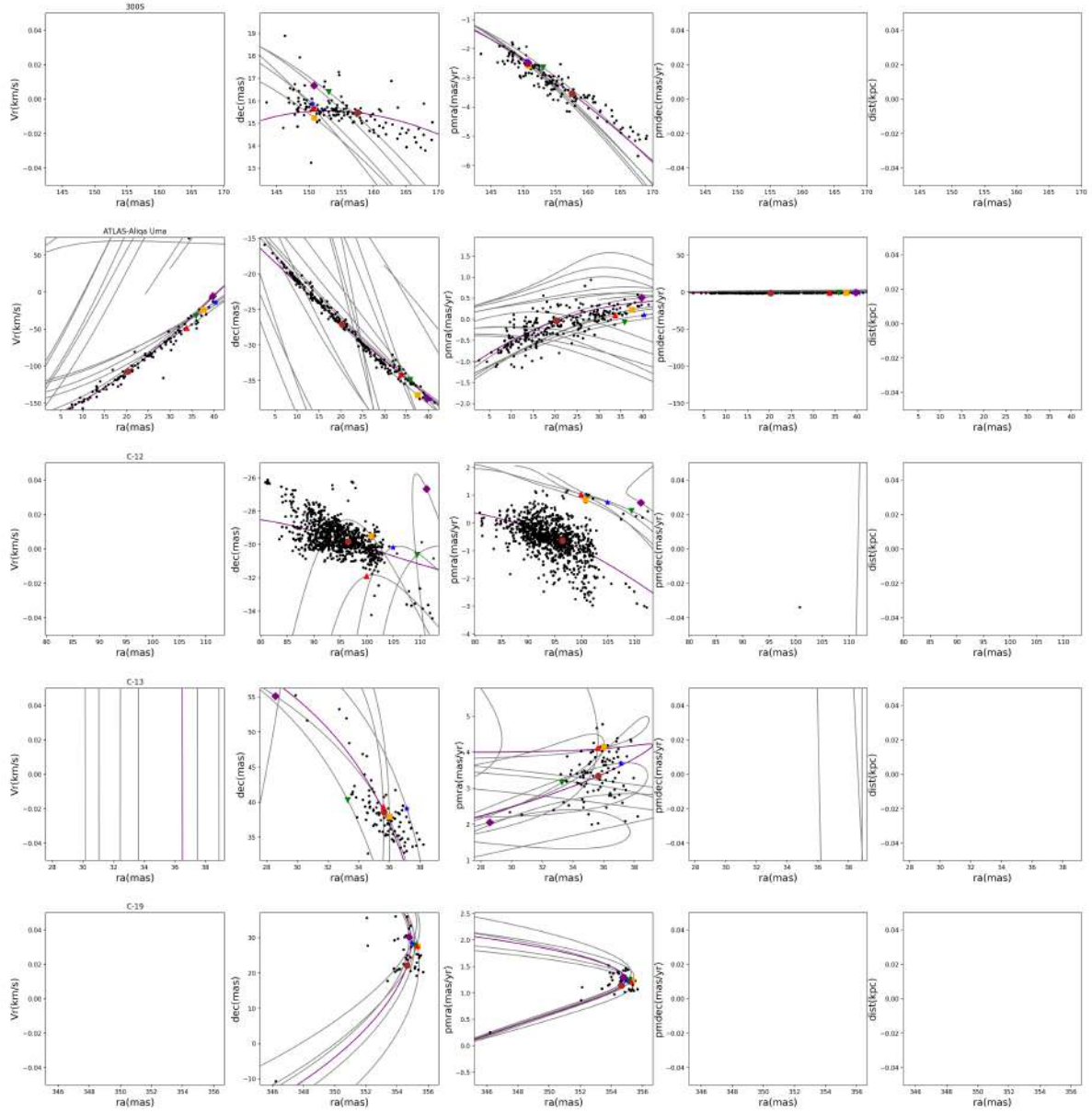

continued.

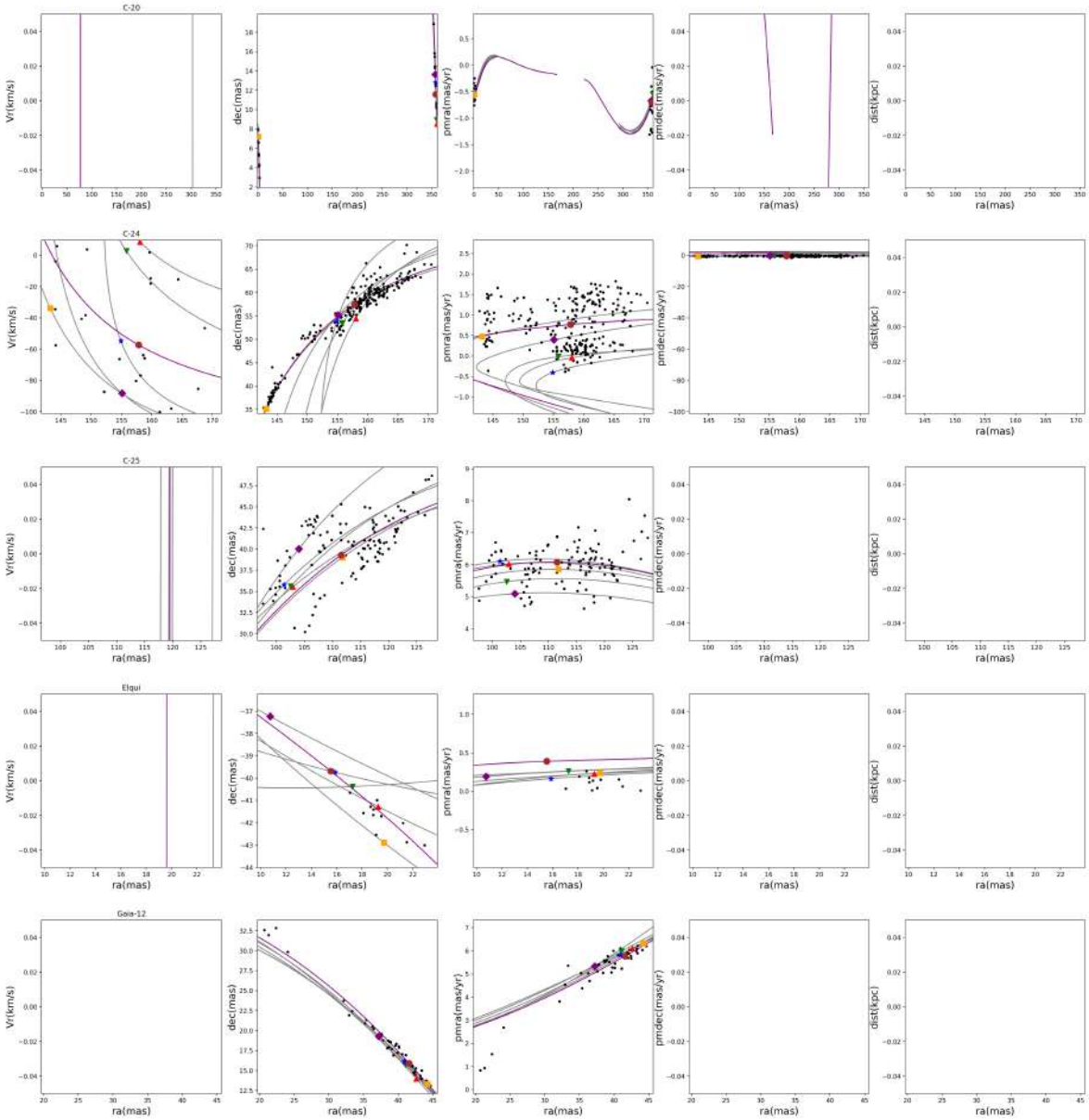
C-20
C-24
C-25
Elqui
Gaia-12
Vr(km/s)
dec(mas)
pmra(mas/yr)
pmdec(mas/yr)
dist(kpc)
ra(mas)

continued.

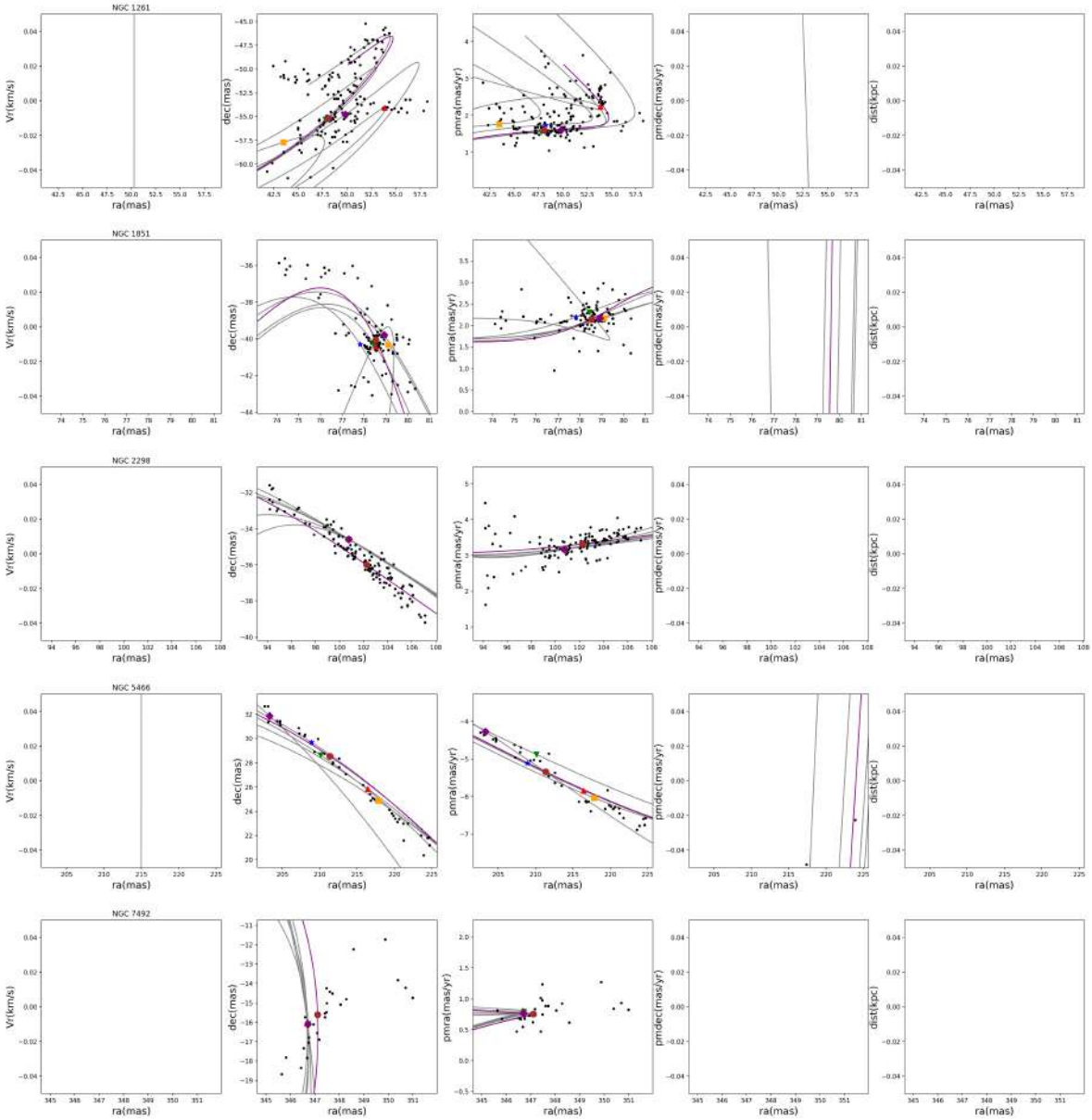
NGC 1261
NGC 1851
NGC 2298
NGC 5466
NGC 7492
Vr(km/s)
dec(mas)
pmra(mas/yr)
pmdec(mas/yr)
dist(kpc)
ra(mas)

continued.

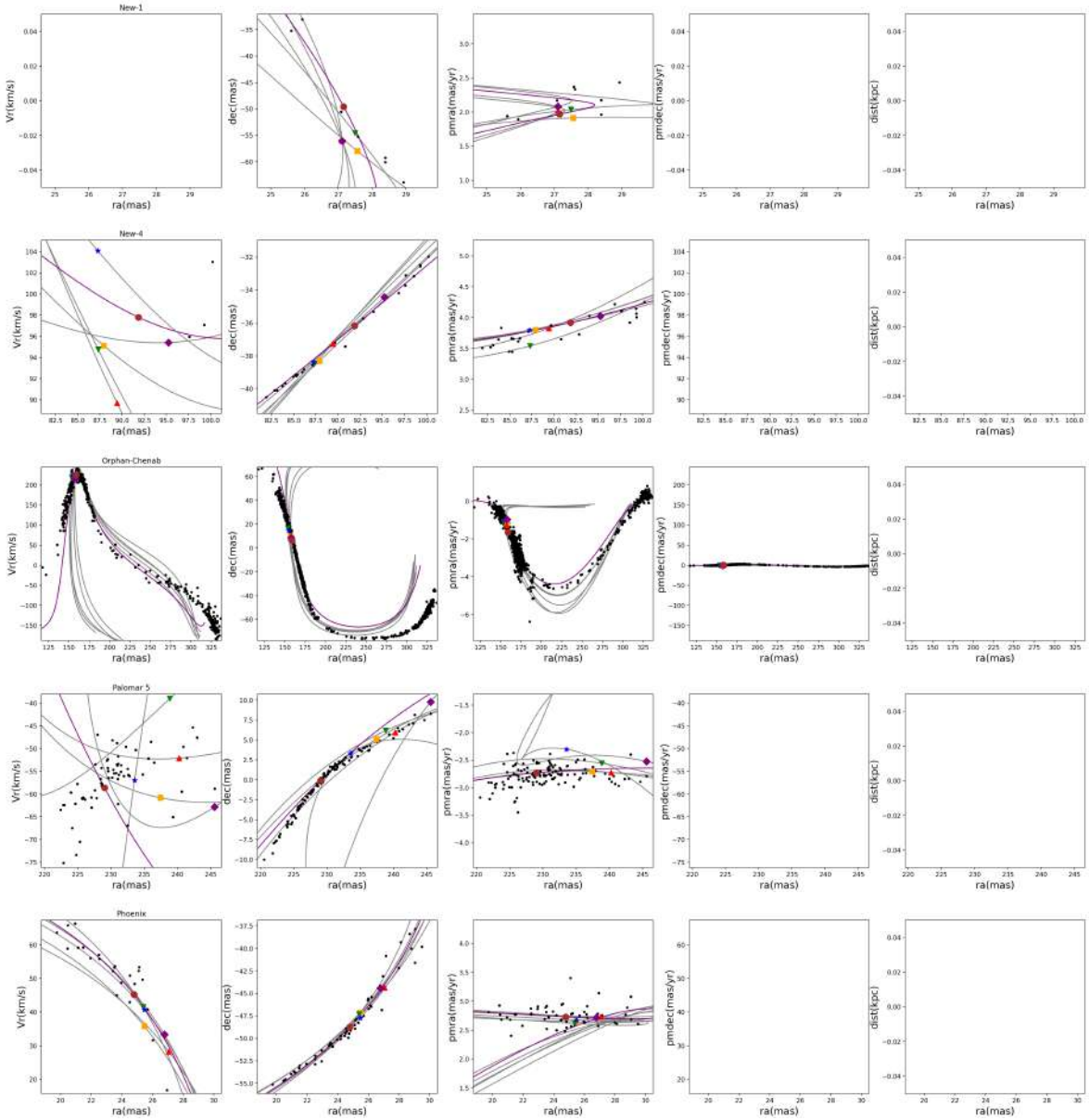
New-1
New-4
Orphan-Chenab
Palomar 5
Phoenix
Vr(km/s)
dec(mas)
pmra(mas/yr)
pmdec(mas/yr)
dist(kpc)
ra(mas)

continued.

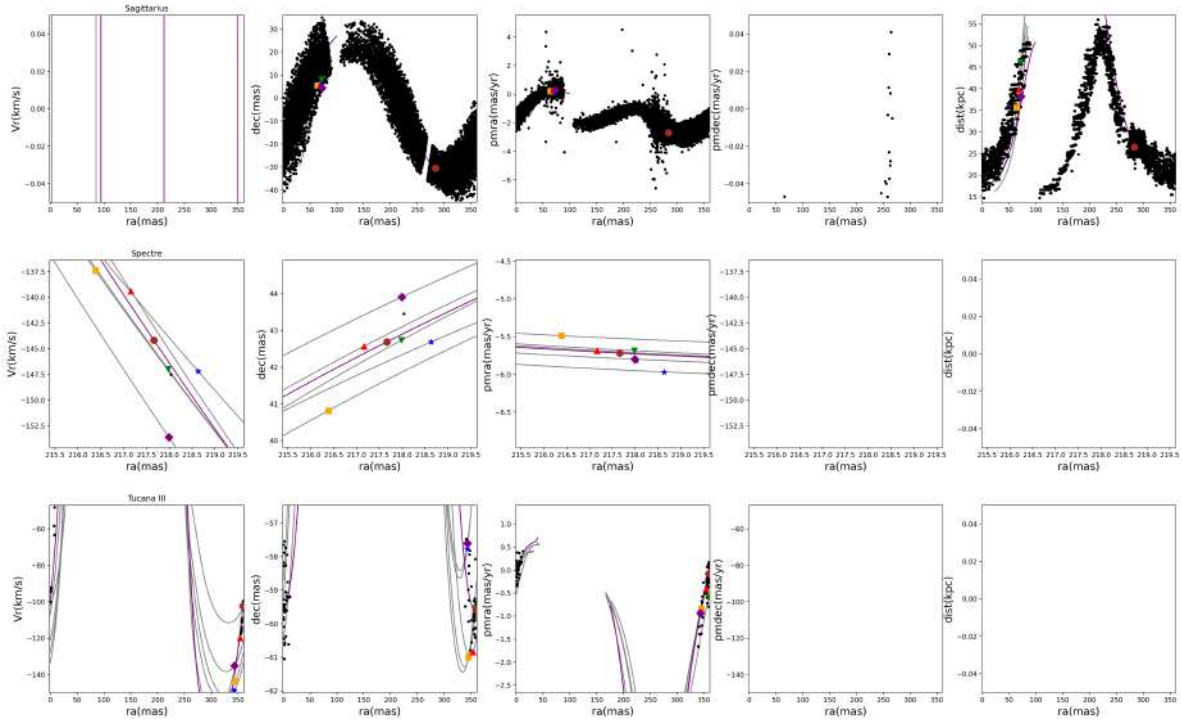
Sagittarius
Spectre
Tucana III
Vr(km/s)
dec(mas)
pmra(mas/yr)
pmdec(mas/yr)
dist(kpc)
ra(mas)

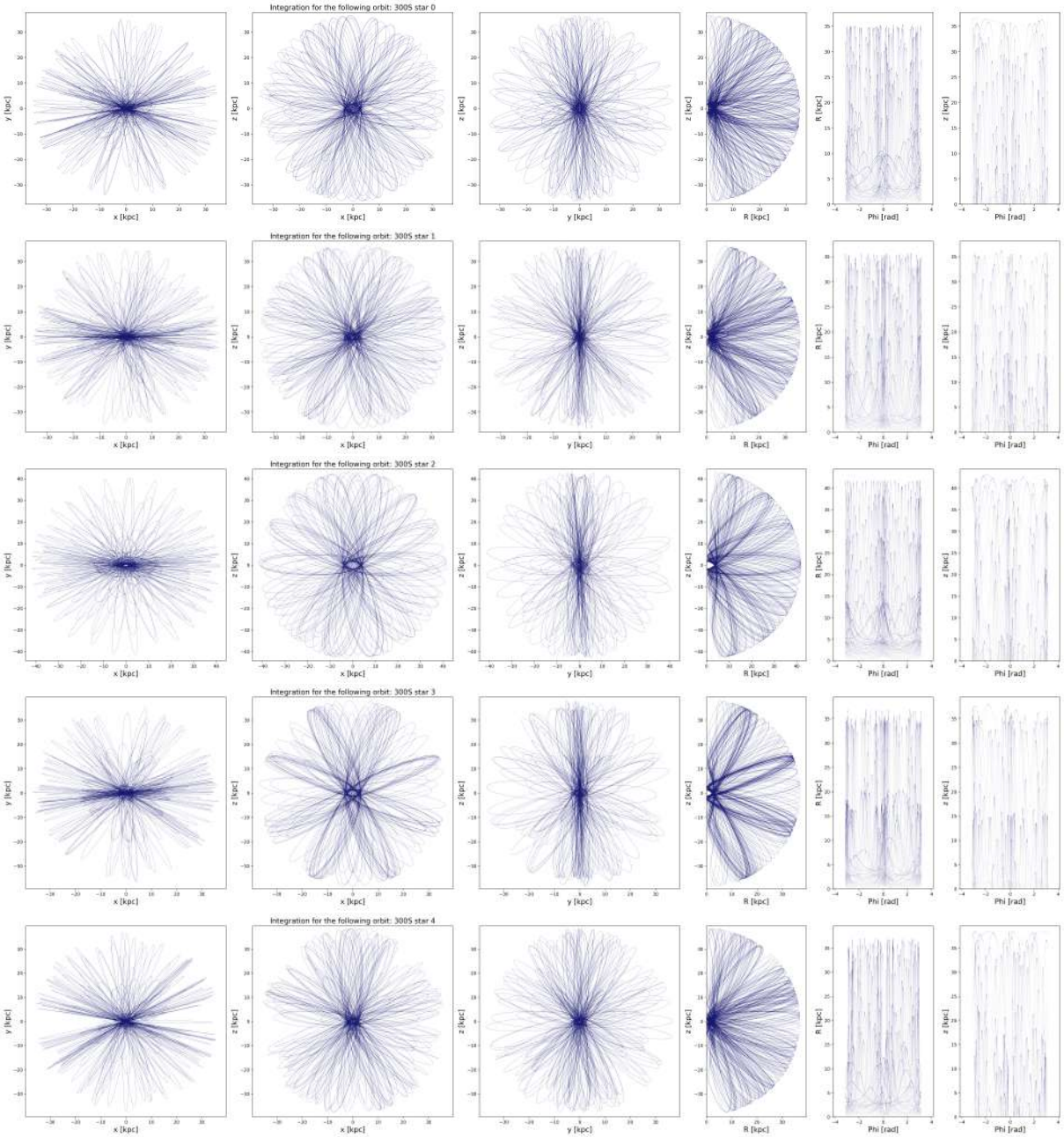

Figure 30: Orbits of candidate members for 300S

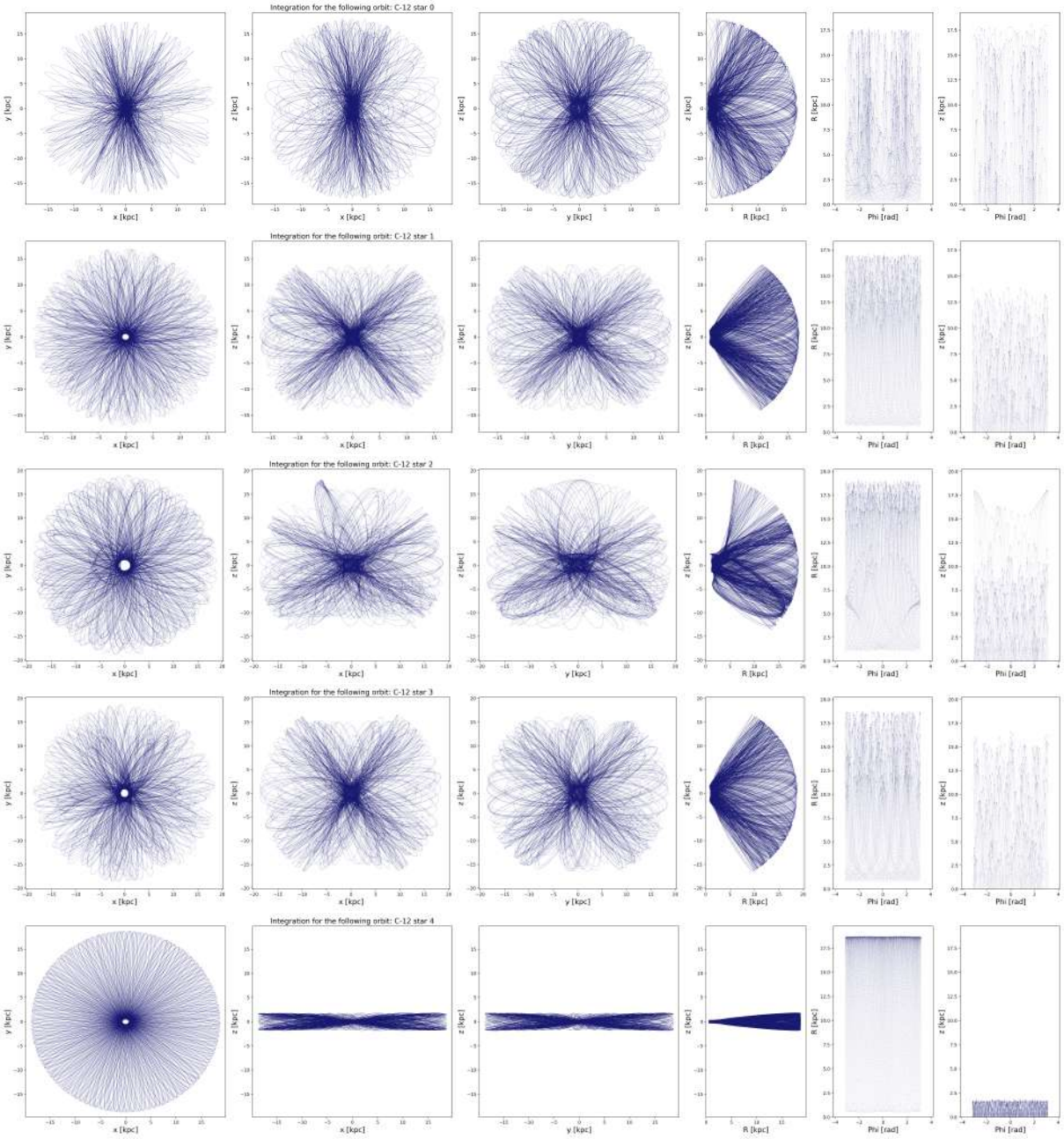

Figure 31: Orbits of candidate members for C-12

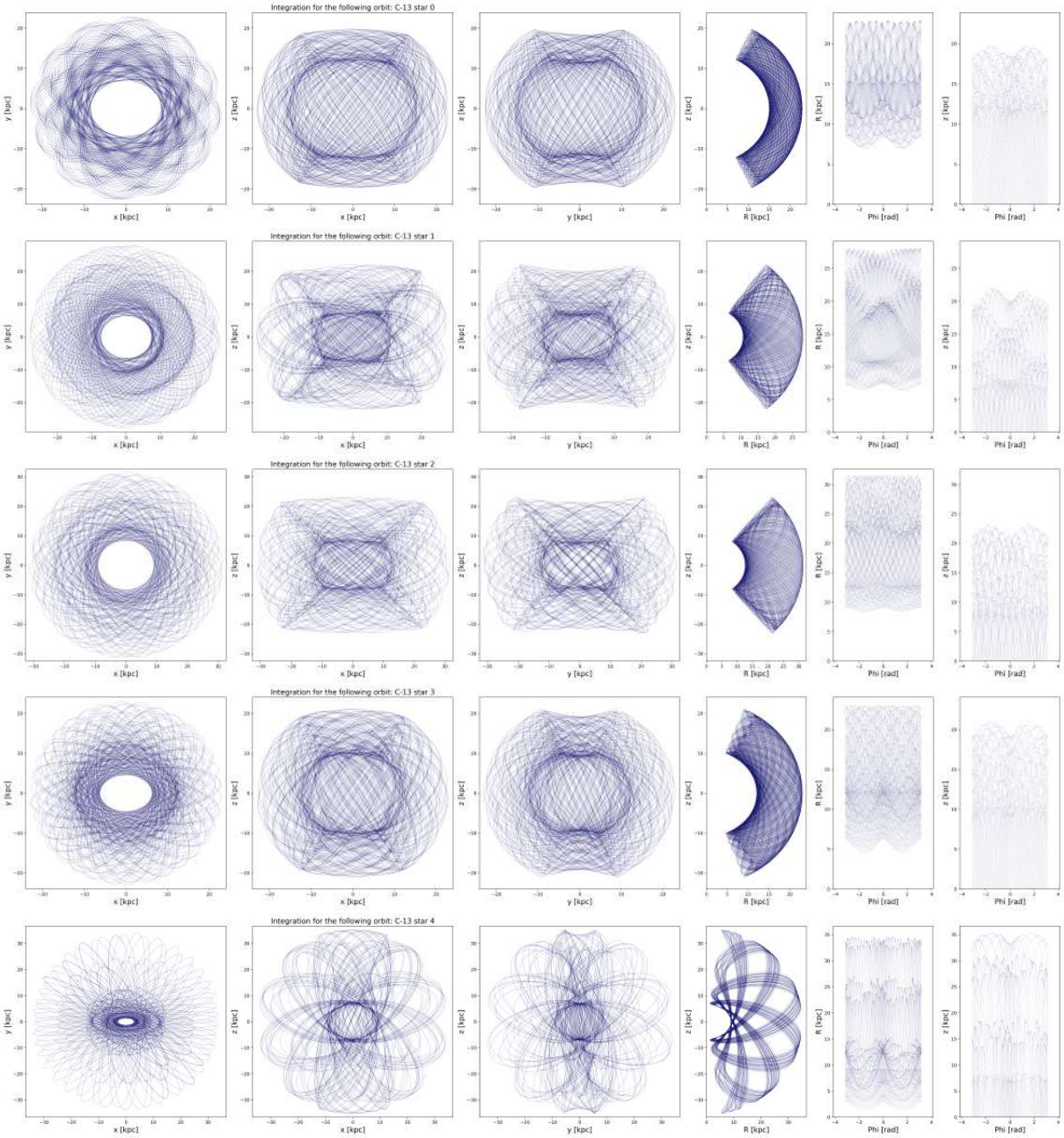

Figure 32: Orbits of candidate members for C-13

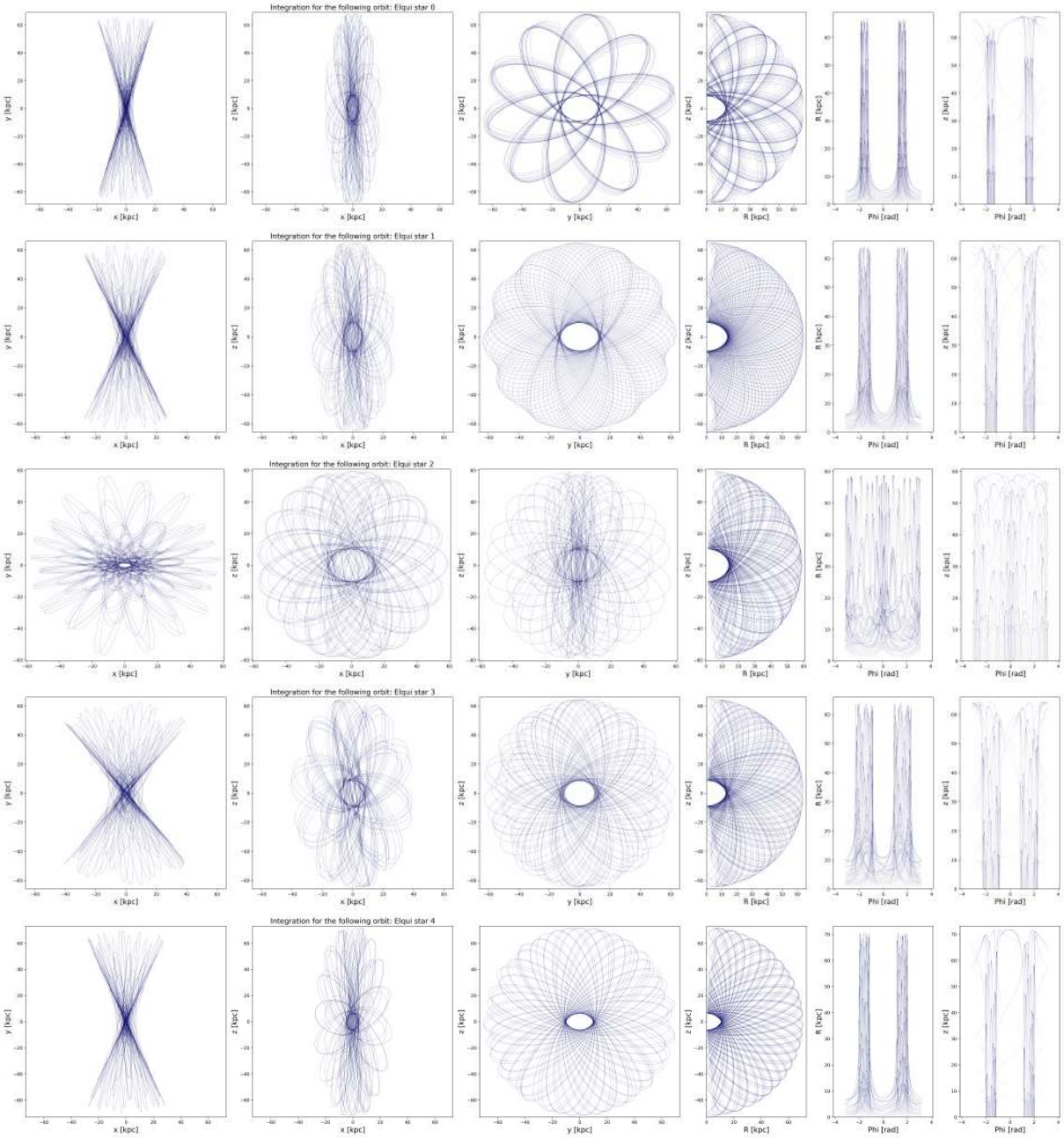

Figure 33: Orbits of candidate members for Elqui

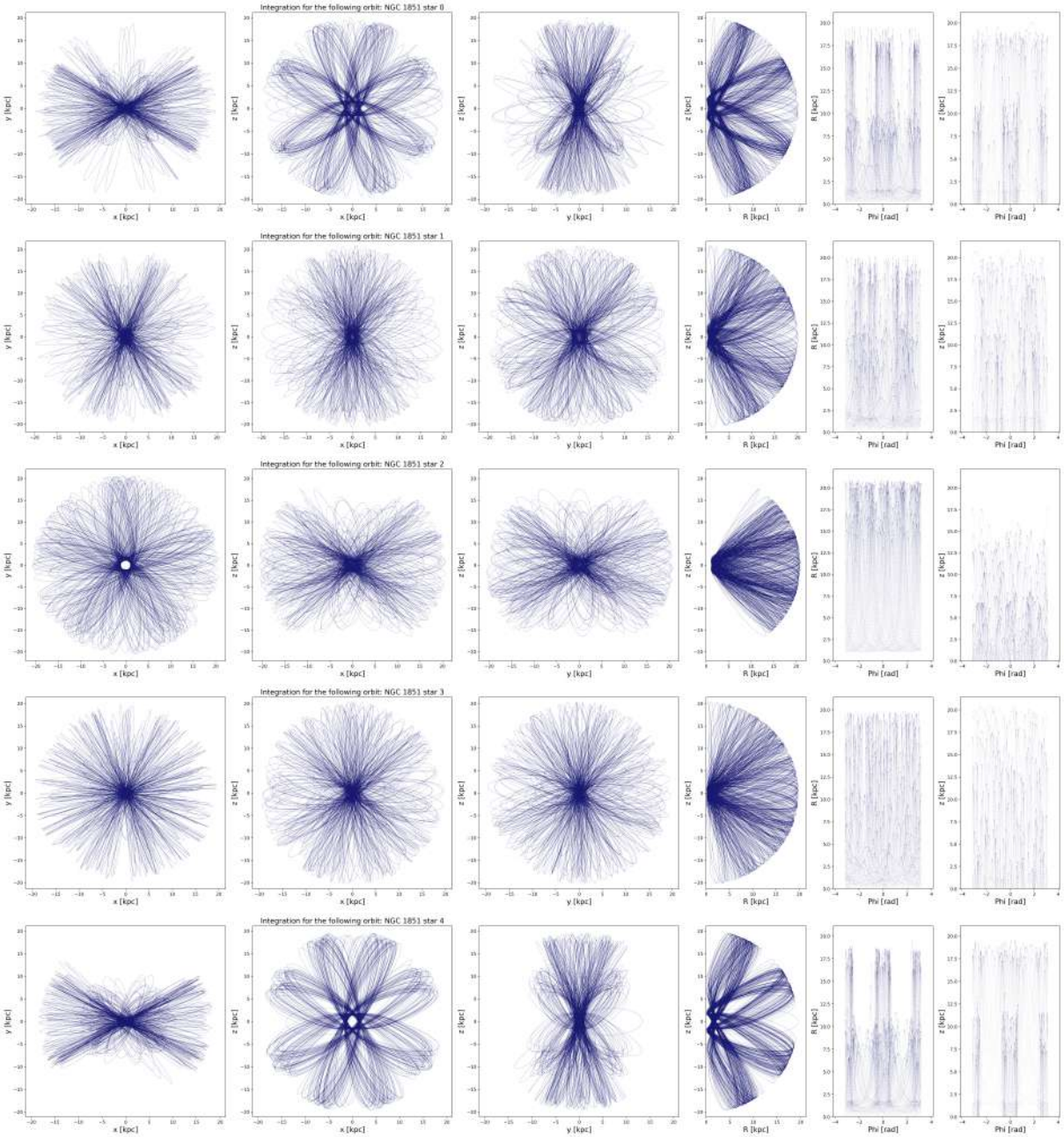

Figure 34: Orbits of candidate members for NGC 1851

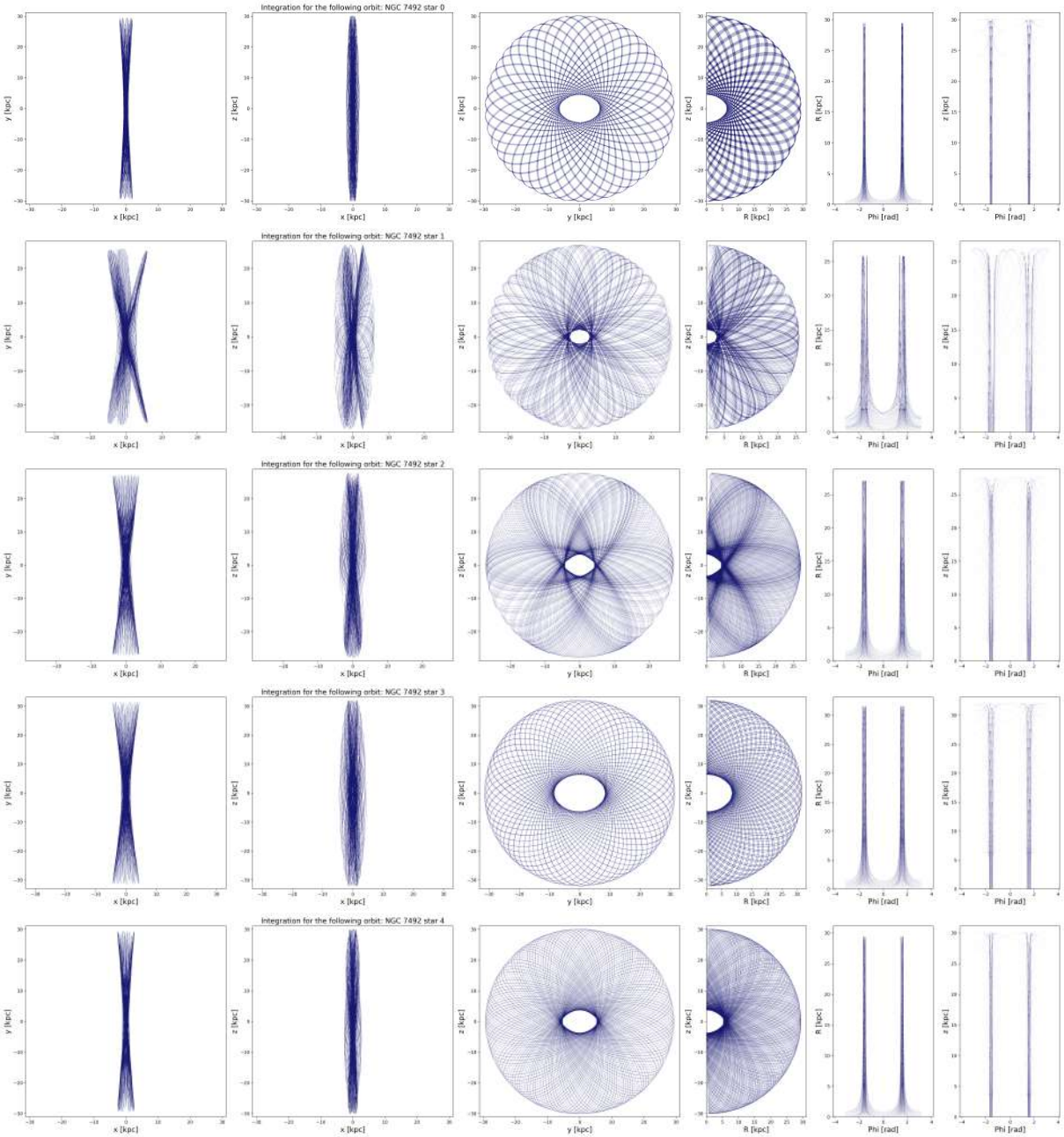

Figure 35: Orbits of candidate members for NGC 7492